6172 *Inorg. Chem.* **2010**, *49*, 6172–6187
DOI: 10.1021/ic100846b

Inorganic Chemistry
Article

Three-Coordinate Terminal Imidoiron(III) Complexes: Structure, Spectroscopy, and Mechanism of Formation

Ryan E. Cowley,[†] Nathan J. DeYonker,[‡] Nathan A. Eckert,[†] Thomas R. Cundari,*[,‡] Serena DeBeer,*[,§] Eckhard Bill,*[,∥] Xavier Ottenwaelder,[⊥] Christine Flaschenriem,[†] and Patrick L. Holland*[,†]

[†]*Department of Chemistry, University of Rochester, Rochester, New York 14627,* [‡]*Department of Chemistry, Center for Advanced Scientific Computing and Modeling (CASCaM), University of North Texas, Denton, Texas 76203,* [§]*Department of Chemistry and Chemical Biology, Baker Laboratory, Cornell University, Ithaca, New York, 14853,* [∥]*Max-Planck-Institut für Bioanorganische Chemie, Mülheim an der Ruhr D45470, Germany, and* [⊥]*Department of Chemistry and Biochemistry, Concordia University, Montreal, Québec H4B 1R6, Canada*

Received April 28, 2010

Reaction of 1-adamantyl azide with iron(I) diketiminate precursors gives metastable but isolable imidoiron(III) complexes LFe═NAd (L = bulky β-diketiminate ligand; Ad = 1-adamantyl). This paper addresses (1) the spectroscopic and structural characterization of the Fe═N multiple bond in these interesting three-coordinate iron imido complexes, and (2) the mechanism through which the imido complexes form. The iron(III) imido complexes have been examined by ^{1}H NMR and electron paramagnetic resonance (EPR) spectroscopies and temperature-dependent magnetic susceptibility (SQUID), and structurally characterized by crystallography and/or extended X-ray absorption fine structure (EXAFS) measurements. These data show that the imido complexes have quartet ground states and short (1.68 $\pm$ 0.01 Å) iron−nitrogen bonds. The formation of the imido complexes proceeds through unobserved iron−N_3R intermediates, which are indicated by QM/MM computations to be best described as iron(II) with an N_3R radical anion. The radical character on the organoazide bends its NNN linkage to enable easy N_2 loss and imido complex formation. The product distribution between imidoiron(III) products and hexazene-bridged diiron(II) products is solvent-dependent, and the solvent dependence can be explained by coordination of certain solvents to the iron(I) precursor prior to interaction with the organoazide.

Introduction

Imido (RN^{2-}) ligands form strong bonds with the transition metals in groups 3−7, particularly those in high formal oxidation states. As a result, imidos often act as unreactive spectator ligands in early metal complexes, for example, in the molybdenum olefin metathesis catalysts of Schrock and co-workers.[1] This strong interaction is a result of π-donation from the two filled nitrogen p orbitals into empty metal d orbitals, which results in a formal bond order of up to three.[2] In late transition metals (groups 8−11), on the other hand, the metal−nitrogen π-interactions are usually destabilized, because in octahedral complexes the antibonding metal dπ and nitrogen pπ orbitals are filled.[3] Thus, late transition metals in the most common geometries typically form weaker bonds with imido fragments, and structurally characterized imido complexes of the late transition metals are uncommon. Though isolating them is difficult, understanding these species is potentially beneficial because the weaker metal−nitrogen bond can enable thermodynamically favorable nitrene transfer to organic compounds, and can also lower the activation barriers to stoichiometric and catalytic reactions. Thus, these "electrophilic" late transition metal imido complexes[4] are of great interest as intermediates in catalytic

*To whom correspondence should be addressed. E-mail: holland@chem.rochester.edu (P.L.H.), Thomas.Cundari@unt.edu (T.R.C.), sdg63@cornell.edu (S.D.), bill@mpi-muelheim.mpg.de (E.B.).

(1) (a) Schrock, R. R. *Chem. Rev.* **2009**, *109*, 3211–3226. (b) Schrock, R. R. *Angew. Chem., Int. Ed.* **2006**, *45*, 3748–3759. (c) Schrock, R. R. *J. Mol. Catal. A: Chem.* **2004**, *213*, 21–30. (d) Schrock, R. R.; Hoveyda, A. H. *Angew. Chem., Int. Ed.* **2003**, *42*, 4592–4633. (e) Schrock, R. R. *Tetrahedron* **1999**, *55*, 8141–8153. (f) Schrock, R. R. *Pure Appl. Chem.* **1994**, *66*, 1447–1454.

(2) (a) Nugent, W. A.; Mayer, J. M. *Metal-Ligand Multiple Bonds*; Wiley: New York, 1988. (b) Wigley, D. E. *Prog. Inorg. Chem.* **1994**, *42*, 239–482.

(3) Mayer, J. M. *Comments Inorg. Chem.* **1988**, *8*, 125–135.

(4) Note that some imide transfer reactions have been achieved with early transition metals, for example: (a) Breslow, R.; Gellman, S. H. *Chem. Commun.* **1982**, 1400–1401. (b) Katsuki, T. *Synlett* **2003**, 281–297. (c) Nishikori, H.; Katsuki, T. *Tetrahedron Lett.* **1996**, *37*, 9245–9248. (d) Noda, K.; Hosoya, N.; Irie, R.; Ito, Y.; Katsuki, T. *Synlett* **1993**, 469–471. (e) Lai, T.-S.; Kwong, H.-L.; Che, C.-M.; Peng, S.-M. *Chem. Commun.* **1997**, 2373–2374. (f) Simonato, J.-P.; Pécaut, J.; Scheidt, R.; Marchon, J.-C. *Chem. Commun.* **1999**, 989–990. (g) Du Bois, J.; Tomooka, C. S.; Hong, J.; Carreira, E. M. *J. Am. Chem. Soc.* **1997**, *119*, 3179–3180. (h) Yu, X.-Q.; Huang, J.-S.; Zhu, N.; Che, C.-M. *Org. Lett.* **2000**, *2*, 2233–2236. (i) Yang, J.; Weinberg, R.; Breslow, R. *Chem. Commun.* **2000**, 531–532. (j) Kohmura, Y.; Katsuki, T. *Tetrahedron Lett.* **2001**, *42*, 3339–3342.

 Published on Web 06/04/2010

nitrene transfer reactions, particularly aminations[5] and aziridinations.[6]

There have been several innovations in stabilizing late transition metal complexes with terminal imido ligands.[7] Stone and co-workers reported in the 1960s and 1970s that several Ir^{I}, Rh^{I}, Ru^{0}, and Os^{0} compounds react with fluoroalkylazides to give crystalline products, and these were formulated as fluoroalkylimido complexes on the basis of IR, NMR, and elemental analysis data.[8] However, these putative imido complexes have never been completely characterized, and the assignments remain in doubt. In the late 1980s and early 1990s, work by Bergman and others generated Os,[9] Ir,[10] and Ru[11] half-sandwich complexes with terminal imido ligands, which were characterized using X-ray crystallography. In the last 10 years, several research groups have published isolable first-row transition metal complexes with terminal imido ligands including those of Fe^{II},[12] Fe^{III},[13] Fe^{IV},[14] Fe^{V},[15] Co^{III},[16] Ni^{II},[17] and Ni^{III}.[18] All of these isolated group 8−10 complexes with terminal imido ligands feature bulky ligands that enforce a coordinatively unsaturated metal center. A low coordination number at the metal has emerged as an important feature, as tetrahedral and trigonal metal centers have π-symmetry orbitals that are not doubly occupied.[19] Thus, even metals with a high formal d-electron count can form stabilizing π-interactions with donors such as NR^{2-} by appropriately manipulating the geometry using the supporting ligands.

The recent successes in isolating late-metal complexes with terminal imido ligands should not lead one to underestimate the difficulty in preparing them. A few have been generated by deprotonation[17a] or hydrogen atom abstraction[16e] from amido complexes, which requires judicious choice of a reagent that can remove the strongly bonded hydrogen without destroying the complex. However, most of the late-metal imido complexes described above arise from the addition of an organoazide to a low-valent, unsaturated metal precursor. This reaction is exothermic and exergonic by virtue of forming N_2 as a byproduct. However, the barrier to breaking the N−N bonds of organoazides is usually high, and the addition of organoazides to late transition metal complexes often leads to an organoazide complex in which the N−N bonds have not been cleaved.[17b,20] Understanding the mechanism and selectivity for N_2 extrusion from metal-organoazide complexes is a current research challenge.[21] Proulx and Bergman invoked a four-centered triazametallacyclobutane

(5) For recent reviews on catalytic C-H amination reactions, see: (a) Müller, P.; Fruit, C. *Chem. Rev.* **2003**, *103*, 2905–2919. (b) Dauban, P.; Dodd, R. H. *Synlett* **2003**, *11*, 1571–1586. (c) Davies, H. M. L.; Long, M. S. *Angew. Chem., Int. Ed.* **2005**, *44*, 3518–3520. (d) Halfen, J. A. *Curr. Org. Chem.* **2005**, *9*, 657–669. (e) Cenini, S.; Gallo, E.; Caselli, A.; Ragaini, F.; Fantauzzi, S.; Piangiolino, C. *Coord. Chem. Rev.* **2006**, *250*, 1234–1253. (f) Compain, P.; Toumieux, S. "Catalytic intramolecular C-H aminations: a powerful tool for the synthesis of various heterocyclic systems," in *Targets in Heterocyclic Systems*; Attanasi, O. A.; Spinelli, D., Eds.; Italian Society of Chemistry: Rome, 2007. (g) Davies, H. M. L.; Manning, J. R. *Nature* **2008**, *451*, 417–424. (h) Von Zezschwitz, P. *Nachr. Chem.* **2008**, *56*, 897–901. (i) Collet, F.; Dodd, R. H.; Dauban, P. *Chem. Commun.* **2009**, 5061–5074. (j) Fantauzzi, S.; Caselli, A.; Gallo, E. *Dalton Trans.* **2009**, 5434–5443.

(6) For recent reviews on aziridines and catalytic aziridination reactions, see: (a) Müller, P.; Fruit, C. *Chem. Rev.* **2003**, *103*, 2905–2919. (b) Halfen, J. A. *Curr. Org. Chem.* **2005**, *9*, 657–669. (c) Tanner, D. *Angew. Chem., Int. Ed. Engl.* **1994**, *33*, 599–619. (d) Osborn, H. M. I.; Sweeney, J. *Tetrahedron: Asymmetry* **1997**, *8*, 1693–1715. (e) Sweeney, J. B. *Chem. Soc. Rev.* **2003**, *31*, 247–258.

(7) Bimetallic group 9−11 complexes featuring bridging imido ligands are also well-studied, for example see: (a) Sharp, P. R.; Ge, Y.-W. *J. Am. Chem. Soc.* **1987**, *109*, 3796–3797. (b) Ge, Y.-W.; Sharp, P. R. *Organometallics* **1988**, *7*, 2234–2236. (c) Ge, Y.-W.; Peng, F.; Sharp, P. R. *J. Am. Chem. Soc.* **1990**, *112*, 2632–2640. (d) Ge, Y.-W.; Sharp, P. R. *J. Am. Chem. Soc.* **1990**, *112*, 3667–3668. (e) Ramamoorthy, V.; Sharp, P. R. *Inorg. Chem.* **1990**, *29*, 3336–3339. (f) Ge, Y.-W.; Sharp, P. R. *Inorg. Chem.* **1992**, *31*, 379–384. (g) Ge, Y.-W.; Sharp, P. R. *Inorg. Chem.* **1993**, *32*, 94–100. (h) Sharp, P. R.; Yi, Y.; Wu, Z.; Ramamoorthy, V. *Spec. Publ. - R. Soc. Chem.* **1993**, *131*, 198–201. (i) Ge, Y.-W.; Ye, Y.; Sharp, P. R. *J. Am. Chem. Soc.* **1994**, *116*, 8384–8385. (j) Ye, C.; Sharp, P. R. *Inorg. Chem.* **1995**, *34*, 55–59. (k) Li, J. J.; Li, W.; James, A. J.; Holbert, T.; Sharp, T. P.; Sharp, P. R. *Inorg. Chem.* **1999**, *38*, 1563–1572. (l) Sharp, P. R. *Comments Inorg. Chem.* **1999**, *21*, 85–114. (m) Sharp, P. R. *Dalton* **2000**, 2647–2657. (n) Anandhi, U.; Holbert, T.; Lueng, D.; Sharp, P. R. *Inorg. Chem.* **2003**, *42*, 1282–1295. (o) Singh, A.; Anandhi, U.; Cinellu, M. A.; Sharp, P. R. *Dalton Trans.* **2008**, 2314–2327. (p) Dobbs, D. A.; Bergman, R. G. *J. Am. Chem. Soc.* **1993**, *115*, 3836–3837. (q) Dobbs, D. A.; Bergman, R. G. *Organometallics* **1994**, *13*, 4594–4605. (r) Danopoulos, A. A.; Wilkinson, G.; Sweet, T. K. N.; Hursthouse, M. B. *J. Chem. Soc., Dalton Trans.* **1996**, 3771–3778. (s) Arita, H.; Ishiwata, K.; Kuwata, S.; Ikariya, T. *Organometallics* **2008**, *27*, 493–496. (t) Ishiwata, K.; Kuwata, S.; Ikariya, T. *J. Am. Chem. Soc.* **2009**, *131*, 5001–5009. (u) Nichols, P. J.; Fallon, G. D.; Murray, K. S.; West, B. O. *Inorg. Chem.* **1988**, *27*, 2795–2800. (v) Ohki, Y.; Takikawa, Y.; Hatanaka, T.; Tatsumi, K. *Organometallics* **2006**, *25*, 3111–3113. (w) Takemoto, S.; Ogura, S.-I.; Yo, H.; Hosokoshi, Y.; Kamikawa, K.; Matsuzaka, H. *Inorg. Chem.* **2006**, *45*, 4871–4873. (x) Zart, M. K.; Powell, D.; Borovik, A. S. *Inorg. Chim. Acta* **2007**, *360*, 2397–2402. (y) Lee, S. W.; Trogler, W. C. *Inorg. Chem.* **1990**, *29*, 1099–1102. (z) Oro, L. A.; Ciriano, M. A.; Tejel, C.; Bordonaba, M.; Graiff, C.; Tiripicchio, A. *Chem.—Eur. J.* **2004**, *10*, 708–715. (aa) Takemoto, S.; Morita, H.; Kamikawa, K.; Matsuzaka, H. *Chem. Commun.* **2006**, 1328–1330. (bb) Allan, R. E.; Beswick, M. A.; Paver, M. A.; Raithby, P. R.; Steiner, A.; Wright, D. S. *Angew. Chem., Int. Ed. Engl.* **1996**, *35*, 208–209. (cc) Reib, P.; Fenske, D. *Z. Anorg. Allg. Chem.* **2000**, *626*, 2245–2247. (dd) Reiss, P.; Fenske, D. *Z. Anorg. Allg. Chem.* **2000**, *626*, 1317–1331. (ee) Badiei, Y. M.; Krishnaswamy, A.; Melzer, M. M.; Warren, T. H. *J. Am. Chem. Soc.* **2006**, *128*, 15056–15057. (ff) Badiei, Y. M.; Dinescu, A.; Dai, X.; Palomino, R. M.; Heinemann, F. W.; Cundari, T. R.; Warren, T. H. *Angew. Chem., Int. Ed.* **2008**, *47*, 9961–9964. (gg) Cundari, T. R.; Dinescu, A.; Kazi, A. B. *Inorg. Chem.* **2008**, *47*, 10067–10072.

(8) (a) Ashley-Smith, J.; Green, M.; Mayne, N.; Stone, F. G. A. *Chem. Commun.* **1969**, 409. (b) McGlinchey, M. J.; Stone, F. G. A. *Chem. Commun.* **1970**, 1265.

(9) Michelman, R. I.; Andersen, R. A.; Bergman, R. G. *J. Am. Chem. Soc.* **1991**, *113*, 5100–5102.

(10) (a) Glueck, D. S.; Hollander, F. J.; Bergman, R. G. *J. Am. Chem. Soc.* **1989**, *111*, 2719–2721. (b) Glueck, D. S.; Wu, J.; Hollander, F. J.; Bergman, R. G. *J. Am. Chem. Soc.* **1991**, *113*, 2041–2054.

(11) (a) Danopoulos, A. A.; Wilkinson, G.; Hussain-Bates, B.; Hursthouse, M. B. *Polyhedron* **1992**, *11*, 2961–2964. (b) Burrell, A. K.; Steedman, A. J. *Organometallics* **1997**, *16*, 1203–1208.

(12) Brown, S. D.; Peters, J. C. *J. Am. Chem. Soc.* **2005**, *127*, 1913–1923.

(13) (a) Brown, S. D.; Betley, T. A.; Peters, J. C. *J. Am. Chem. Soc.* **2003**, *125*, 322–323. (b) Betley, T. A.; Peters, J. C. *J. Am. Chem. Soc.* **2003**, *125*, 10782–10783. (c) Bart, S. C.; Lobkovsky, E.; Bill, E.; Chirik, P. J. *J. Am. Chem. Soc.* **2006**, *128*, 5302–5303. (d) Mehn, M. P.; Brown, S. D.; Jenkins, D. M.; Peters, J. C.; Que, L. *Inorg. Chem.* **2006**, *45*, 7417–7427. (e) Lu, C. C.; Saouma, C. T.; Day, M. W.; Peters, J. C. *J. Am. Chem. Soc.* **2007**, *129*, 4–5. (f) Scepaniak, J. J.; Young, J. A.; Bontchev, R. P.; Smith, J. M. *Angew. Chem., Int. Ed.* **2009**, *48*, 3158–3160.

(14) (a) Verma, A. K.; Nazif, T. N.; Achim, C.; Lee, S. C. *J. Am. Chem. Soc.* **2000**, *122*, 11013. (b) Thomas, C. M.; Mankad, N. P.; Peters, J. C. *J. Am. Chem. Soc.* **2006**, *128*, 4956–4957. (c) Nieto, I.; Ding, F.; Bontchev, R. P.; Wang, H.; Smith, J. M. *J. Am. Chem. Soc.* **2008**, *130*, 2716–2717.

(15) Ni, C.; Fettinger, J. C.; Long, G. J.; Brynda, M.; Power, P. P. *Chem. Commun.* **2008**, 6045–6047.

(16) (a) Jenkins, D. M.; Betley, T. A.; Peters, J. C. *J. Am. Chem. Soc.* **2002**, *124*, 11238–11239. (b) Hu, X.; Meyer, K. *J. Am. Chem. Soc.* **2004**, *126*, 16322–16323. (c) Dai, X.; Kapoor, P.; Warren, T. H. *J. Am. Chem. Soc.* **2004**, *126*, 4798–4799. (d) Shay, D. T.; Yap, G. P. A.; Zakharov, L. N.; Rheingold, A. L.; Theopold, K. H. *Angew. Chem., Int. Ed.* **2005**, *44*, 1508-1510; erratum: 2006, 45, 7870. (e) Cowley, R. E.; Bontchev, R. P.; Sorrell, J.; Sarracino, O.; Feng, Y.; Wang, H.; Smith, J. M. *J. Am. Chem. Soc.* **2007**, *129*, 2424–2425. (f) Jones, C.; Schulten, C.; Rose, R. P.; Stasch, A.; Aldridge, S.; Woodul, W. D.; Murray, K. S.; Moubaraki, B.; Brynda, M.; La Macchia, G.; Gagliardi, L. *Angew. Chem., Int. Ed.* **2009**, *48*, 7406–7410.

(17) (a) Mindiola, D. J.; Hillhouse, G. L. *J. Am. Chem. Soc.* **2001**, *123*, 4623–4624. (b) Waterman, R.; Hillhouse, G. L. *J. Am. Chem. Soc.* **2008**, *130*, 12628–12629.

(18) Kogut, E.; Wiencko, H. L.; Zhang, L.; Cordeau, D. E.; Warren, T. H. *J. Am. Chem. Soc.* **2005**, *127*, 11248–11249.

(19) Holland, P. L. *Acc. Chem. Res.* **2008**, *41*, 905–914.

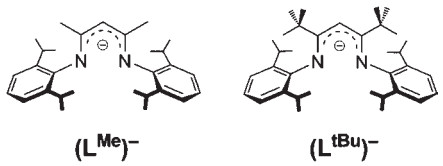

Figure 1. β-Diketiminate ligands used in this study.

intermediate to explain how a coordinated phenylazide ligand extruded N_2 to afford an imidotantalum complex.[20b] Recent density functional theory (DFT)-based simulations have also addressed possible mechanisms for N_2 loss from organoazide complexes.[22] Hillhouse recently described the isolation of a nickel-organoazide complex that loses N_2 to form an imidonickel complex upon warming.[17b]

In this contribution, evidence is presented for the formation of a transient formally iron(I) organoazide complex on the way to an isolable iron(III) imido complex. In a novel feature, the metal-N_3R species has significant radical character on the organoazide ligand. It is shown that the addition of donor ligands controls the selectivity between several potential products obtained from organoazide addition. In addition, the geometric and electronic structure of the first structurally characterized three-coordinate iron(III) imido complex is explored in detail using crystallography, electron paramagnetic resonance (EPR), NMR, magnetic susceptibility, X-ray absorption, and computational chemistry techniques. These combined studies lead to new insight about the mechanism of formation of a late-metal imido complex, as well as its bonding and charge distribution.

Results

Products from Iron(I) and Adamantyl Azide. The diiron dinitrogen complexes $L^RFeNNFeL^R$ ($L^R = L^{Me}$ or L^{tBu}, Figure 1) have been shown to be convenient sources of the evanescent two-coordinate iron(I) fragment "LFe" in reactions with alkynes, alkenes, CO, isocyanides, S_8, phosphines, and benzo[*c*]cinnoline.[23b,24] Therefore, it was hypothesized that $L^{Me}FeNNFeL^{Me}$ and $L^{tBu}FeNNFeL^{tBu}$ would serve as useful iron(I) precursors in building imidoiron(III) complexes. However, addition of 2 equiv of 1-adamantyl azide

Scheme 1

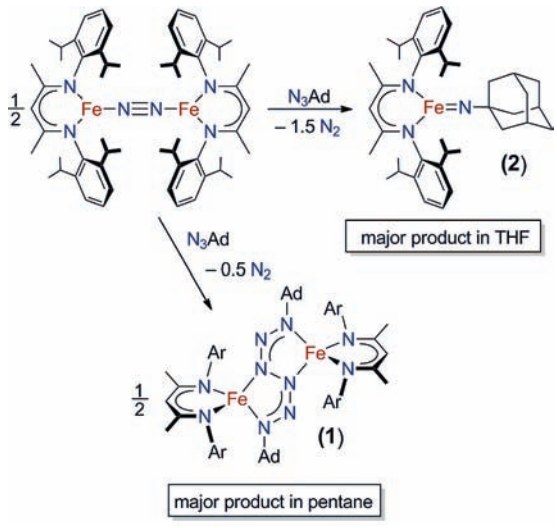

Table 1. Solvent Dependence of the Outcome of the Reaction between $L^{Me}FeNNFeL^{Me}$ and 2.0 equiv N_3Ad[a]

solvent	yield of **1** (%)[b]	yield of **2** (%)[c]	approximate ratio **2**:**1**[d]
pentane	77	14	1:6
Et_2O	64	25	1:3
2,5-dimethyl-THF	63	28	1:2
toluene	52	41	1:1
benzene	47	43	1:1
$PhCF_3$	20	59	3:1
pentane +4 equiv of 4-^{t}Bu-pyridine	10	68	7:1
THF	9	80	9:1

[a] Each reaction performed at [Fe] = 15 mM. [b] Isolated powder. [c] Detected in ^{1}H NMR spectrum of crude reaction product. [d] Rounded to the nearest whole number in the ratio.

(N_3Ad) to a pentane solution of $L^{Me}FeNNFeL^{Me}$ *did not* produce the imido complex as the major product, but instead led to an unusual "hexazene" complex $L^{Me}Fe(\mu\text{-}\eta^2\text{:}\eta^2\text{-AdNNNNNNAd-}1\kappa^2N^1,N^4\text{:}2\kappa^2N^3,N^6)FeL^{Me}$ (**1**) in 74% yield (Scheme 1).[25] This product is conceptually derived from addition of two "$L^{Me}Fe$" fragments to two molecules of N_3Ad or, alternatively, the dimerization of two $L^{Me}Fe(N_3Ad)$ complexes. The characterization of **1** was reported recently, and Mössbauer spectroscopy and magnetic studies were used to show that **1** is best described as being composed of two iron(II) centers and a dianionic $[Ad_2N_6]^{2-}$ ligand.[25] Therefore, **1** derives from reductive coupling of two N_3Ad groups through their terminal nitrogen atoms. The related compound $L^{Me}Mg(\mu\text{-}\eta^2\text{:}\eta^2\text{-AdNNNNNNAd})MgL^{Me}$ was recently reported by Jones, Stasch, and co-workers, and it was similarly prepared through reductive coupling of N_3Ad by the magnesium(I) precursor $L^{Me}MgMgL^{Me}$.[26]

When performing the above reaction in pentane, signals for the desired $L^{Me}FeNAd$ (**2**) (characterized below) are observed in the ^{1}H NMR spectrum of crude reaction mixtures, but **2** is formed in only 14% yield. The relative amounts of **1** and **2** are highly dependent on the solvent used in the reaction (Table 1). In each reaction, the

(20) (a) Proulx, G.; Bergman, R. G. *J. Am. Chem. Soc.* **1995**, *117*, 6382–6383. (b) Proulx, G.; Bergman, R. G. *Organometallics* **1996**, *15*, 684–692. (c) Fickes, M. G.; Davis, W. M.; Cummins, C. C. *J. Am. Chem. Soc.* **1995**, *117*, 6384–6385. (d) Guillemot, G.; Solari, E.; Floriani, C.; Rizzoli, C. *Organometallics* **2001**, *20*, 607–615. (e) Dias, H. V. R.; Polach, S. A.; Goh, S.-K.; Archibong, E. F.; Marynick, D. S. *Inorg. Chem.* **2000**, *39*, 3894–3901. (f) Hanna, T. A.; Baranger, A. M.; Bergman, R. G. *Angew. Chem., Int. Ed. Engl.* **1996**, *35*, 653–655. (g) Barz, M.; Herdtweck, E.; Thiel, W. R. *Angew. Chem., Int. Ed.* **1998**, *37*, 2262–2265. (h) Albertin, G.; Antoniutti, S.; Baldan, D.; Castro, J.; García-Fontán, S. *Inorg. Chem.* **2008**, *47*, 742–748.

(21) Cenini, S.; La Monica, G. *Inorg. Chim. Acta* **1976**, *18*, 279–293.

(22) (a) Wu, H.; Hall, M. B. *J. Am. Chem. Soc.* **2008**, *130*, 16452–16453. (b) Cundari, T. R.; Morello, G. R. *J. Org. Chem.* **2009**, *74*, 5711–5714.

(23) (a) Smith, J. M.; Lachicotte, R. J.; Pittard, K. A.; Cundari, T. R.; Lukat-Rodgers, G.; Rodgers, K. R.; Holland, P. L. *J. Am. Chem. Soc.* **2001**, *123*, 9222–9223. (b) Smith, J. M.; Sadique, A. R.; Cundari, T. R.; Rodgers, K. R.; Lukat-Rodgers, G.; Lachicotte, R. J.; Flaschenriem, C. J.; Vela, J.; Holland, P. L. *J. Am. Chem. Soc.* **2006**, *128*, 756–769.

(24) (a) Vela, J.; Stoian, S.; Flaschenriem, C. J.; Münck, E.; Holland, P. L. *J. Am. Chem. Soc.* **2004**, *126*, 4522–4523. (b) Stoian, S. A.; Yu, Y.; Smith, J. M.; Holland, P. L.; Bominaar, E. L.; Münck, E. *Inorg. Chem.* **2005**, *44*, 4915–4922. (c) Yu, Y.; Smith, J. M.; Flaschenriem, C. J.; Holland, P. L. *Inorg. Chem.* **2006**, *45*, 5724–5751. (d) Yu, Y.; Sadique, A. R.; Smith, J. M.; Dugan, T. R.; Cowley, R. E.; Brennessel, W. W.; Flaschenriem, C. J.; Bill, E.; Cundari, T. R.; Holland, P. L. *J. Am. Chem. Soc.* **2008**, *130*, 6624–6638. (e) Sadique, A. R.; Brennessel, W. W.; Holland, P. L. *Inorg. Chem.* **2008**, *47*, 784–786.

(25) Cowley, R. E.; Elhaïk, J.; Eckert, N. A.; Brennessel, W. W.; Bill, E.; Holland, P. L. *J. Am. Chem. Soc.* **2008**, *130*, 6074–6075.

(26) Bonyhady, S. J.; Green, S. P.; Jones, C.; Nembenna, S.; Stasch, A. *Angew. Chem., Int. Ed.* **2009**, *48*, 2973–2977.

hexazene complex **1** is poorly soluble, and thus the yield of **1** was easily determined by filtration of the crude reaction mixture. The yield of imido complex **2** was determined based on ^{1}H NMR integration against an internal standard. The yield of imido **2** was lowest (< 30%) in non-coordinating solvents (pentane, diethyl ether, and 2,5-dimethyltetrahydrofuran (Me_2THF)), intermediate (40−68%) in aromatic solvents (benzene, toluene, and α,α,α-trifluorotoluene ($PhCF_3$)), and highest (80%) in THF. In each of these reactions, the combined yields of hexazene **1** and imido **2** was 79−93% based on iron.[27]

Because it gave the highest conversion to **2**, tetrahydrofuran (THF) was chosen for the isolation of pure samples of **2**. Addition of a THF solution of N_3Ad to a royal purple solution of 0.5 equiv of $L^{Me}FeNNFeL^{Me}$ in THF produces vigorous effervescence and an immediate color change to deep yellow. Removal of THF and crystallization of the residue from pentane at low temperature produced a yellow-brown crystalline product in 61% isolated yield. Crystals of **2** are stable for more than 2 weeks in the solid state at −45 °C, and this level of stability enabled spectroscopic and crystallographic characterization. At 25 °C, C_6D_6 solutions of redissolved crystals of **2** are metastable with $t_{1/2} \sim 48$ h. We initially reported the generation of **2** in the presence of 4-*tert*-butylpyridine (^{t}Bupy), but under these conditions $t_{1/2}$ was only about 0.5 h at 25 °C, and crystallographic characterization was not possible.[28]

X-ray Crystal Structure of 2. Single crystals of **2** were grown from a saturated pentane solution at −45 °C, and the X-ray crystal structure is shown in Figure 2a. The short Fe=N bond length (1.6699(15) Å) and nearly linear geometry at nitrogen ($\angle_{Fe=N-C}$ = 170.40(13)°) highlight the Fe=N multiple bond character. These values are in the range observed in known terminal imidoiron compounds for Fe=N bond lengths (1.61−1.73 Å) and Fe=N−C angles (159−179°).[29] The three-coordinate iron center is planar (sum of N−Fe−N angles is 360.0(1)°), and slightly bent from ideal Y-shaped geometry, as evidenced by the difference in N_{imido}=Fe−$N_{diketiminate}$ angles (126.82(6)° and 139.16(6)°). The Fe−$N_{diketiminate}$ bond lengths (1.9285(13), 1.9177(13) Å) are significantly shorter than those in three-coordinate iron(II) diketiminate complexes (average 1.98(2) Å),[30] consistent with the assignment of the iron oxidation state in **2** as iron(III).

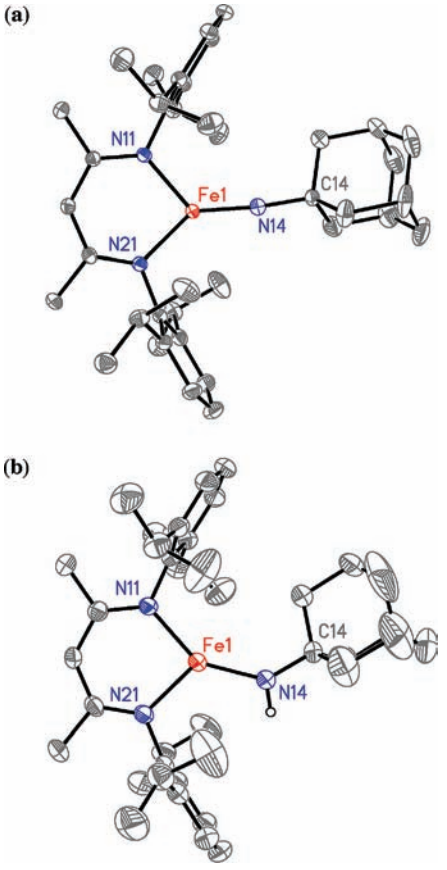

Figure 2. Molecular structures of (a) $L^{Me}Fe$=NAd (**2**), and (b) $L^{Me}Fe$−NHAd (**3**) using 50% probability thermal ellipsoids. Hydrogen atoms except the amido hydrogen are omitted. Selected bond distances [Å] and bond angles [deg] for $L^{Me}Fe$=NAd (**2**): Fe1−N14, 1.6699(15); Fe1−N11, 1.9285(13); Fe1−N21, 1.9177(13), Fe1−N14−C14, 170.40(13); N11−Fe1−N14, 139.16(6); N21−Fe1−N14, 126.82(6); N11−Fe1−N21, 94.02(6). Selected bond distances [Å] and bond angles [deg] for $L^{Me}Fe$-NHAd (**3**): Fe1−N14, 1.860(2); Fe1−N11, 1.974(2); Fe1−N21, 1.986(2), Fe1−N14−C14, 134.7(2); N11−Fe1−N14, 145.86(8); N21−Fe1−N14, 121.04(8); N11−Fe1−N21, 93.09(7).

The structure of the iron(III) imido complex can be compared to the analogous iron(II) amido complex L^{Me}-FeNHAd (**3**) (Figure 2b), which can be generated independently via anion metathesis of $[L^{Me}FeCl]_2$ with 2 equiv of LiNHAd in a manner similar to other (*β*-diketiminato)-Fe^{II}(amido) complexes.[31] The Fe−N_{amido} distance of 1.841(2) Å in **3** is typical of its congeners with NH(*p*-tolyl), NH(2,6-diisopropylphenyl), and NH(^{t}Bu) ligands,[31] and is 0.171(3) Å longer than the Fe=N multiple bond in **2**. The geometry at iron in the structure of **3** is midway between Y-shaped and T-shaped, with N_{imido}=Fe−$N_{diketiminate}$ angles of 145.88(8)° and 121.03(8)°. Also, the Fe−$N_{diketimipate}$ lengths in **3** (1.974(2) and 1.985(2) Å) are ∼0.05 Å longer than the corresponding bond lengths in **2** because of the lower oxidation state, and are consistent with other three-coordinate iron(II) diketiminate complexes.[30]

(27) During the synthesis of **2** from $L^{Me}FeNNFeL^{Me}$ and 2 equiv N_3Ad, trace amounts (2−5%) of the tetrazene complex $L^{Me}Fe(AdNNNNAd-\kappa^2N^1N^4)$ (**5**) are unavoidably present in crude reaction mixtures, presumably because the cycloaddition reaction of **2** with AdN_3 is kinetically competitive with imido formation. Fortunately, **5** is much less soluble in pentane than **2**, and extraction of the crude material into pentane is usually sufficient to reduce the amount of **5** contaminant in **2** to < 1%, as judged by ^{1}H NMR spectroscopy. Also, note that **5** was originally obtained by reaction of **2**·^{t}**Bupy** with 1 equiv of N_3Ad (see reference 48). We have noticed that the reaction proceeds qualitatively faster when base-free **2** is used instead of **2**·^{t}**Bupy**, consistent with a mechanism that involves rate-limiting ^{t}Bupy dissociation to form **2**, and subsequent cycloaddition of N_3Ad to the Fe=N bond. Complex **5** can be also obtained in 81% yield in one step from $L^{Me}FeNNFeL^{Me}$ and 4 equiv N_3Ad in THF, without the use of pyridine in the reaction. Details of this simplified synthesis are given in the Experimental Section.

(28) Eckert, N. A.; Vaddadi, S.; Stoian, S.; Lachicotte, R. J.; Cundari, T. R.; Holland, P. L. *Angew. Chem., Int. Ed.* **2006**, *45*, 6868–6871.

(29) The average Fe=N bond length is 1.65(3) Å, and the average Fe=N−C angle is 173(5)°, calculated from the 15 imidoiron compounds with terminal imido ligands in the Cambridge Structural Database, v. 5.30 (Feb 2009 update). Allen, F. H. *Acta Crystallogr.* **2002**, *B58*, 380–388.

(30) The large library of 3- and 4-coordinate iron−diketiminate complexes in the Cambridge Crystallographic Structure Database has allowed us to determine average Fe−$N_{diketiminate}$ bond lengths as a function of coordination number and oxidation state; see SI for details.

(31) Eckert, N. A.; Smith, J. M.; Lachicotte, R. J.; Holland, P. L. *Inorg. Chem.* **2004**, *43*, 3306–3321.

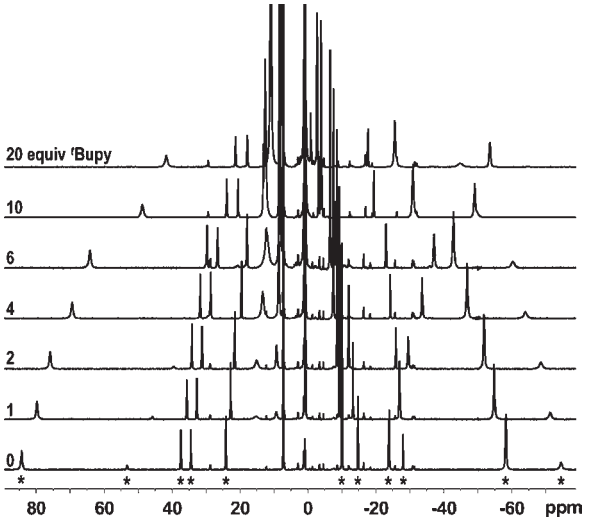

Figure 3. ^{1}H NMR spectra of **2** (C_6D_6, 25 °C) at the specified concentrations of ^{t}Bupy. The 11 peaks assigned to **2** (marked with *) are indicated in the bottom spectrum. The small peaks with δ_H independent of [^{t}Bupy] are due to trace contamination with the iron-tetrazene complex **5**.[27]

Scheme 2

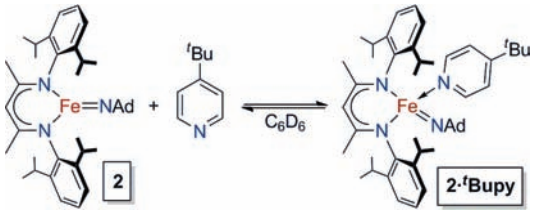

Coordination of Lewis Bases to the Imido Complex 2. The ability of THF to steer the reaction between L^{Me}-FeNNFeL^{Me} and N_3Ad toward the imidoiron(III) product **2** suggests that Lewis bases are beneficial. Consistent with this idea, performing the reaction in pentane in the presence of at least 4 equiv of ^{t}Bupy gave a much higher yield of **2** and less than 10% of **1** (Table 1). To investigate the equilibrium between **2** and **2·^{t}Bupy** (Scheme 2), we added 1−20 equiv of ^{t}Bupy to a C_6D_6 solution of **2** that had been previously crystallized. When ^{t}Bupy was added, the color immediately changed from yellow-brown to dark red-orange. The ^{1}H NMR spectrum of the mixture showed 11 paramagnetic peaks qualitatively similar to that of pyridine-free **2**, as well as three broad peaks that are consistent with ^{t}Bupy coordination. In contrast, addition of 100 equiv of THF to a C_6D_6 solution of **2** did not shift the ^{1}H NMR resonances more than 0.2 ppm or produce a color change, suggesting that THF does not coordinate to **2**.

The positions of all peaks in the ^{1}H NMR spectra of mixtures of **2** and ^{t}Bupy are dependent on the concentration of ^{t}Bupy (Figure 3), indicating that there is an equilibrium between three-coordinate L^{Me}FeNAd (**2**) and four-coordinate L^{Me}Fe(NAd)(^{t}Bupy) (**2·^{t}Bupy**) that is rapid on the ^{1}H NMR time scale. To confirm this hypothesis, the in situ-generated **2·^{t}Bupy** was treated with a stoichiometric amount of BPh_3 to scavenge the Lewis base from solution. This treatment shifted the paramagnetic ^{1}H NMR resonances for **2·^{t}Bupy** to become identical to those in crystallized **2**, and the exchange-broadened

Scheme 3

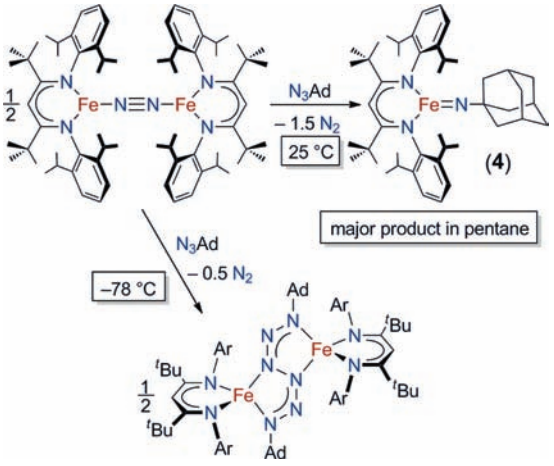

^{t}Bupy peaks at δ 15.1 and δ 9.3 ppm disappeared (Supporting Information, Figure S-2). Five aromatic ^{1}H NMR resonances were observed (δ 6.4 to 8.3 ppm), consistent with the formation of the borane−pyridine adduct ^{t}Bupy·BPh_3.[32]

The solutions of **2·^{t}Bupy** were unstable because the four-coordinate species undergoes intramolecular hydrogen atom abstraction (HAA) from the isopropyl C−H of the diketiminate ligand, with $t_{1/2}$ on the order of ~0.5 h at 25 °C. This HAA reaction was reported previously,[28] and mechanistic details of this reaction shall be explored in detail elsewhere.[33] The addition of BPh_3 to solutions of **2·^{t}Bupy** greatly improved the stability of the complex, as $t_{1/2}$ for decomposition of the mixture increased to ~36 h at 25 °C, similar to that for **2** prepared in THF and without ^{t}Bupy.

Effect of Diketiminate Size on the Outcome of the Reaction. We also investigated the imidoiron complex supported by the bulkier L^{tBu} ligand. This imido complex was obtained by adding 2 equiv of N_3Ad to a solution of L^{tBu}FeNNFeL^{tBu} (Scheme 3). At room temperature in pentane, the target imidoiron(III) complex L^{tBu}FeNAd (**4**) was generated in >80% spectroscopic yield,[34] which differs significantly from the low conversion to the L^{Me} analogue **2** (14% yield of imido in pentane). The hexazene complex {L^{tBu}Fe}$_2$(Ad_2N_6) is also formed, but only in <2% crude yield. Larger amounts of hexazene complex (>20% isolated) were only obtained when the reaction was performed at −78 °C.[25] Therefore, the use of the bulkier L^{tBu} ligand greatly decreases the formation of the hexazene byproduct.

Although we have not been able to obtain single crystals of **4** for crystallography, the assignment of **4** is supported by NMR spectroscopy. As shown in Figure 4, the ^{1}H NMR spectra of **2** and **4** are qualitatively very similar, suggesting they have similar geometries and electronic structures. The most significant difference between the two spectra is the chemical shift of the peaks attributed to the different ligand backbone substituent

(32) The same compound "^{t}Bupy·BPh_3" is obtained from ^{t}Bupy + BPh_3 in the absence of any Fe complex; see SI for details.

(33) Cowley, R. E.; Eckert, N. A.; Vaddadi, S.; Figg, T.; Cundari, T. R.; Holland, P. L. manuscript in preparation.

(34) Cowley, R. E.; Eckert, N. A.; Elhaïk, J.; Holland, P. L. *Chem. Commun.* **2009**, 1760–1762.

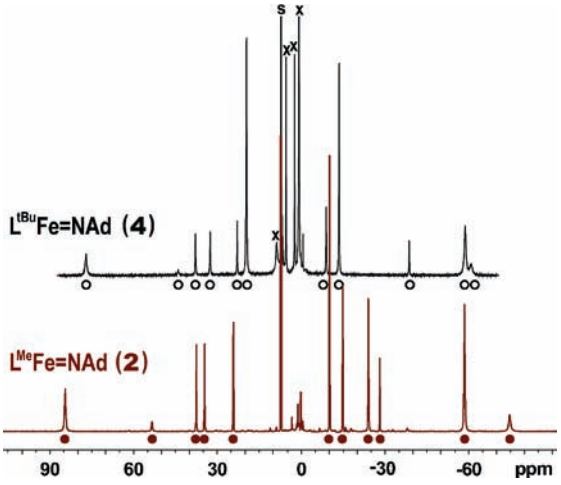

Figure 4. ^{1}H NMR spectra for **2** (bottom) and **4** (top)[34] on the same scale. The 11 peaks assigned to each complex are marked with filled circles (**2**) or open circles (**4**). Residual solvent signals are marked with "s". The spectrum of **4** is recorded in the presence of excess 1,4-cyclohexadiene and 4-*tert*-butylpyridine (marked with "x") to show that it does not react.

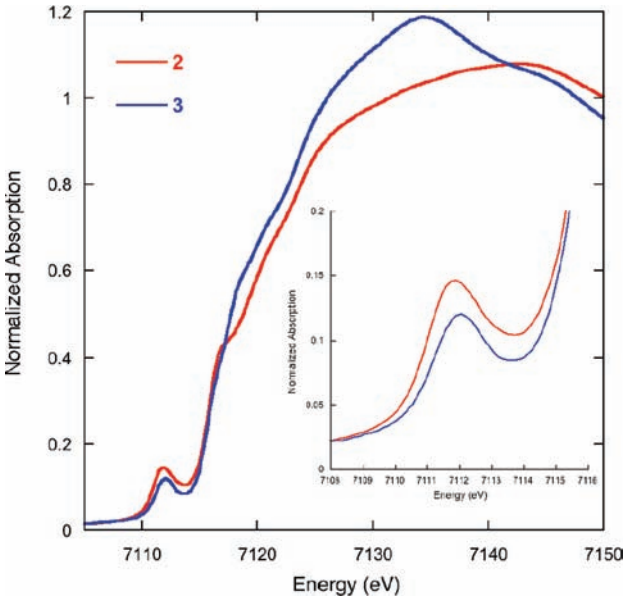

Figure 5. Comparison of the normalized Fe K-edge XAS data for **2** and **3**. The inset shows the pre-edge feature at greater magnification.

(Me in **2** at δ −24 ppm; ^{t}Bu in **4** at δ +20 ppm). The similarity between features in the X-band EPR spectra and extended X-ray absorption fine structure (EXAFS) fits of **2** and **4** will also become evident below.

In other ways, compound **4** differs from **2**. L^{tBu}FeNAd (**4**) does not coordinate exogenous donors such as ^{t}Bupy, and does not react with H$^\bullet$ sources such as 1,4-cyclohexadiene or indene that react with **2**.[28] Despite its greater steric protection, **4** is less stable than **2** in solution, decomposing to a mixture of products with $t_{1/2}$ of approximately 1 h at 25 °C. Therefore, it has been handled only in solution at low temperatures. However, we have been able to isolate a solid containing L^{tBu}FeNAd in 50−70% purity for EXAFS measurements (see below). The nature of the decomposition products is unknown.

EXAFS Characterization of Imido Complexes. To further confirm the identity of the two imido complexes,

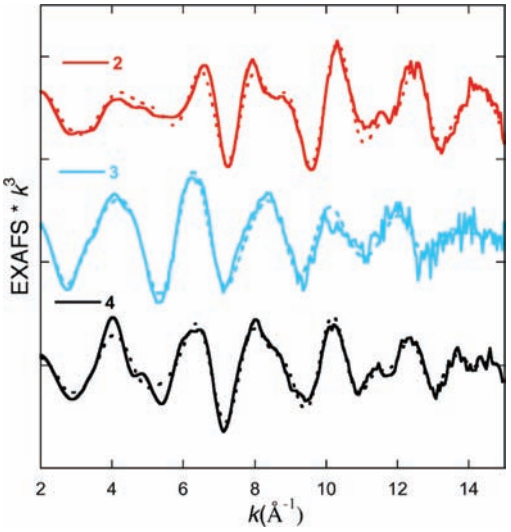

Figure 6. k^3-weighted EXAFS data and the corresponding fits for **2**, **3**, and **4**.

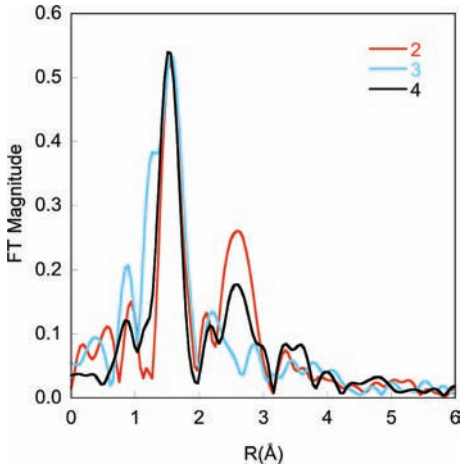

Figure 7. Non-phase shift corrected FT (Fourier transformed) data for **2**, **3**, and **4**.

we obtained Fe K-edge X-ray absorption spectroscopy (XAS) data on imidoiron(III) complexes **2** and **4**, as well as on the amidoiron(II) complex **3**. XAS data for each compound were obtained in the solid state as dilutions in boron nitride.[35] A comparison of the Fe K-edges for **2** and **3** are shown in Figure 5. The rising edge is at higher energy in the imidoiron(III) complex **2** than in the amidoiron(II) complex **3**, consistent with the higher oxidation state. There is essentially no change in the pre-edge energies on going from **2** to **3**, but the pre-edge intensity is somewhat larger for **2** than **3**. A tentative interpretation is that the overall ligand field is similar, but there is greater covalency in the imido complex **2**.

The EXAFS data for **2**, **3**, and **4** (together with the corresponding fits) are shown in Figure 6. The non-phase-shift-corrected Fourier-transformed (FT) data are shown in Figure 7. The overall EXAFS beat pattern, as well as the FTs, for imido complexes **2** and **4** are very similar. On the other hand, for the amido complex **3** there is a

(35) Frozen solutions gave somewhat different spectra, probably from greater decomposition. See Supporting Information for details.

Table 2. EXAFS Fit Results

2			3			4		
	r (Å)	σ^2 (Å^2)		r (Å)	σ^2 (Å^2)		r (Å)	σ^2 (Å^2)
2 Fe−N	1.94	0.0039	3 Fe−N/O	2.00	0.0067	2.5 Fe−N	1.99	0.0062
1 Fe−N	1.69	0.0052				0.5 Fe−N	1.69	0.0045
6 Fe−N−C	2.89	0.0038	6 Fe−N−C	2.97	0.0075	6 Fe−N−C	2.91	0.0028
ΔE_0 (eV)	−8.60		ΔE_0 (eV)	−4.45		ΔE_0 (eV)	−7.71	
error[a]	0.079		error[a]	0.189		error[a]	0.069	

[a] Error is given by $\sum[(\chi_{obsd} - \chi_{calcd})^2 k^6]/\sum[(\chi_{obsd}{}^2 k^6]$.

distinctly different beat pattern and a broader first shell feature in the FT. The data for **2** were successfully modeled with two nitrogen atoms at 1.94 Å, and one nitrogen atom at 1.69 Å (Table 2). These are assigned as $Fe-N_{diketiminate}$ and $Fe{=}N_{imido}$ bonds since they closely match the corresponding bond lengths from the crystal structure (1.93 and 1.67 Å, respectively). The fit was significantly poorer if the short Fe=N distance was omitted from the model, with the error increasing from 0.079 to 0.316. Although there is no distinct peak in the Fourier-transformed spectrum that corresponds to the short Fe−N scatterer, a similar trend has been noted for other complexes with short Fe−N bonds; the lack of a distinct peak arises from an interference effect that results in a narrower peak in the FT in the presence of a short Fe−N vector (see Figure 7).[36] Hence, the EXAFS data corroborate the short Fe=N distance observed in the X-ray crystal structure.[37]

The EXAFS data for **4** are of particular interest because this compound has not been subjected to crystallographic characterization. In this case, the data fit to 2.5 nitrogen atoms at 1.99 Å and 0.5 nitrogen atoms at 1.69 Å, distances similar to those in the fit for **2**. Inclusion of 1 Fe−N at 1.69 Å resulted in an unreasonably large σ^2 value (0.032 Å^2), suggesting that the imido complex **4** represents only ~1/2 of the species present. Since **4** was not purified through crystallization and is less stable than **2**, it is not surprising that the imido complex is less pure. However, the EXAFS data for **2** and **4** are still quite similar, and both show short (< 1.7 Å) Fe=N distances, suggesting that they both contain imido ligands.

Magnetism of 2. We previously described the X-band EPR spectra of solution-generated **4**[34] and **2·^{t}Bupy**.[38] The rhombic signal for each of these compounds is similar (g_{eff} = 7.0, 1.8, 1.3 for **4**; g_{eff} = 6.1, 1.9, 1.4 for **2·^{t}Bupy**) and indicates an S = 3/2 spin system with $E/D \sim 0.33$. The X-band EPR spectrum of a solution of pyridine-free, crystalline **2** (Supporting Information, Figure S-11) was very similar (g_{eff} = 6.3, 1.9, 1.5) to that reported previously for **2·^{t}Bupy**,[28] showing that **2** and **^{t}Bupy** interact very weakly, as indicated also by the NMR experiments described above.

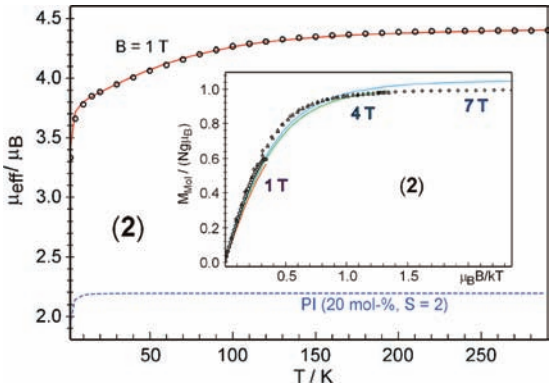

Figure 8. Variable-temperature magnetic susceptibility of crystalline **2** recorded with a field of B = 1 T. The solid red line represents the best fit achieved by adding the values for 20% of an unknown paramagnetic impurity with S = 2, D = 2 cm^{-1}, g_{av} = 2 to the result of a spin Hamiltonian simulation (PI, dotted blue line, assuming same molar mass). The optimized simulation parameters for the target compound with S = 3/2 are g_{av} = 2.15, $|D|$ = 65 cm^{-1}, and E/D = 0.33. Inset: Multiple-field variable-temperature measurements at B = 1, 4, and 7 T and simulation with the same parameters (red, green, and blue traces, respectively).

Crystalline **2** was also evaluated by magnetic susceptibility measurements. The variable-temperature magnetic susceptibility data (μ_{eff}) for solid **2** are shown in Figure 8. The high-temperature limit, corresponding to an effective magnetic moment of ~4.6 μ_B, exceeds the spin-only value for S = 3/2 (3.87 μ_B), but it is consistent with the effective magnetic moment measured in C_6D_6 solution (Evans method, 25 °C) of μ_{eff} = 4.4 ± 0.3 μ_B. The deviation is most likely due to the presence of an unknown paramagnetic contaminant, which is EPR-silent. In previous Mössbauer studies of **2·^{t}Bupy**, variable amounts of iron(II) impurities were observed,[28] and some decomposition is expected because of the metastable nature of **2**. By assuming that the impurity is an iron(II) species in 20% abundance with spin S = 2 and roughly the same molar mass, the magnetic data could be successfully fitted to an S = 3/2 model with g_{av} = 2.15 and $|D|$ = 65(5) cm^{-1}, and E/D = 0.33. The rhombicity parameter of E/D = 0.33 was taken from simulations of the EPR spectrum mentioned above, whereas D and the average g value were refined to fit the magnetic susceptibility data. The refinement gave g = 2.15, which is close to that found for the EPR solution sample (g_{av} = 2.07). The remarkably large value for D was corroborated by variable-temperature measurements at multiple fields (inset of Figure 8). Although the global fit of these traces using the same parameters and including the same S = 2 impurity is not

(36) (a) Aliaga-Alcalde, N.; DeBeer George, S.; Mienert, B.; Bill, E.; Wieghardt, K.; Neese, F. *Angew. Chem., Int. Ed.* **2005**, *44*, 2908–2912. (b) Berry, F.; Bill, E.; Bothe, E.; DeBeer George, S.; Mienert, B.; Neese, F.; Wieghardt, K. *Science* **2006**, *312*, 1937–1941.

(37) It is also important to note that the EXAFS data of the amido complex **3** show no evidence of a short Fe−N bond; the data are best fit by inclusion of three Fe−N interactions at 2.00 Å. Attempts to separate the first shell into shorter 1.8 Å and longer 2.0 Å components, as indicated by the crystal structure, resulted in the two distance components converging to the same value. This suggests that the separation of these components is beyond the resolution of the EXAFS data.

(38) The EPR signal assigned to **2** in reference 28 was present in ~70% yield based on integration.

perfect, it shows clearly that the very small nesting of isofield curves can be reproduced only with $|D| > 50$ cm^{-1} for $E/D \approx 0.3$ (or $-D > 35$ cm^{-1} for free $E/D = 0$), because only with such large zero-field splitting are the m_s-sublevels of the $S = 3/2$ manifold sufficiently isolated to exhibit the observed field-independent behavior of the magnetization curves $M(\mu_B B/kT)$.[39] In summary, the ability to fit both EPR and magnetic data to a self-consistent quartet model strongly supports a description of **2** having an $S = 3/2$ ground state. This conclusion is also consistent with the quartet spin state being lowest by 10 kcal/mol in DFT computations.[28]

Computations On a Putative Iron(I)-Adamantylazide Intermediate. Next, we considered the mechanism through which $L^{Me}FeNNFeL^{Me}$ might form **1** and **2**. Because $L^{Me}FeNNFeL^{Me}$ reacts with Lewis bases to form monomeric iron(I) adducts $L^{Me}Fe$(Lewis base),[23b,24b−24d] it is reasonable to hypothesize a 1:1 adduct $L^{Me}Fe(N_3Ad)$ as the first species formed. Other transition metal−organoazide complexes thermally convert to metal−imido complexes.[17b,20a−c] No intermediate species are observed by ^{1}H NMR spectroscopy during the very rapid reaction of the iron-N_2 complex with N_3Ad, even at cold temperatures. Therefore, the characteristics and reactions of the putative organoazide species were evaluated using quantum mechanics/molecular mechanics (QM/MM) computations with classical treatment (Universal Force Field) of the 2,6-diisopropylphenyl and methyl substituents of the β-diketiminate ligand and the adamantyl group with the exception of the carbon atom that is directly bonded to nitrogen. The core of the complex was modeled via density functional theory (DFT) at the B3LYP/6-311+G(d) level of theory. All doublet states were considerably higher in energy (> 13 kcal/mol) than quartet and sextet states, and are not described here.

Azide Coordination Mode in $L^{Me}Fe(N_3Ad)$. Since N_3Ad is known to bind metals in three different coordination modes (Figure 9), we first sought to identify the lowest-energy linkage isomer of $L^{Me}Fe(N_3Ad)$ and elucidate its electronic structure. Isomers of $L^{Me}Fe(N_3Ad)$ were evaluated with the azide group bonded at the internal nitrogen ($L^{Me}Fe(N_3Ad\text{-}\kappa N^1)$), the terminal nitrogen ($L^{Me}Fe(N_3Ad\text{-}\kappa N^3)$), and side-on ($L^{Me}Fe(\eta^2\text{-}N_3Ad)$), in both quartet (IS) and sextet (HS) spin states. The triazametallacyclobutene isomer $L^{Me}Fe(N_3Ad\text{-}\kappa^2 N^1,N^3)$ was also evaluated, but quartet and sextet models were each found to be considerably (> 30 kcal/mol) higher in energy than the other low-energy linkage isomers, and were not considered further.

The optimized geometries for the lowest spin state of each isomer are shown in Figure 10, and the relative energies of all isomer/spin state combinations are summarized in Table 3. Though sextet $L^{Me}Fe(N_3Ad\text{-}\kappa N^1)$ is the lowest energy linkage isomer, the $L^{Me}Fe(N_3Ad\text{-}\kappa N^3)$ and $L^{Me}Fe(\eta^2\text{-}N_3Ad)$ linkage isomers are close in energy (lowest spin states +5.0 and +7.1 kcal/mol relative to $^6L^{Me}Fe(N_3Ad\text{-}\kappa N^1)$). In mechanistic discussions below, we shall assume that the different low-energy linkage isomers can interconvert easily.

Geometry and Electronic Structure of $L^{Me}Fe(N_3Ad)$. The calculated Fe−N_{azido} bond length in $^6L^{Me}Fe(N_3Ad\text{-}\kappa N^1)$ is

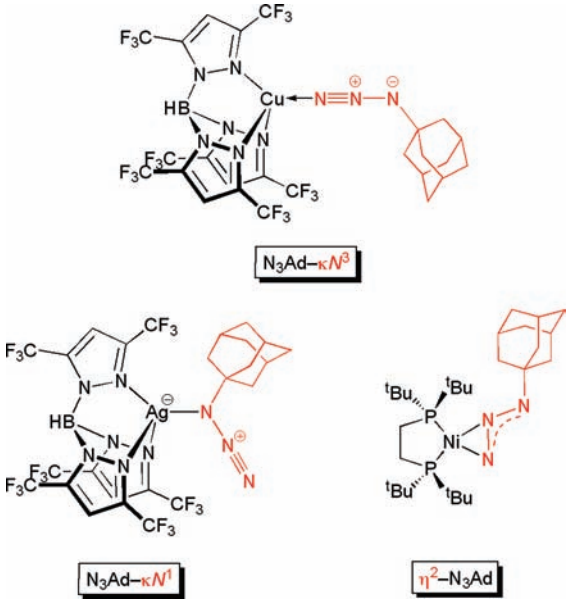

Figure 9. Examples of different coordination modes of N_3Ad from literature complexes.[17b,40c]

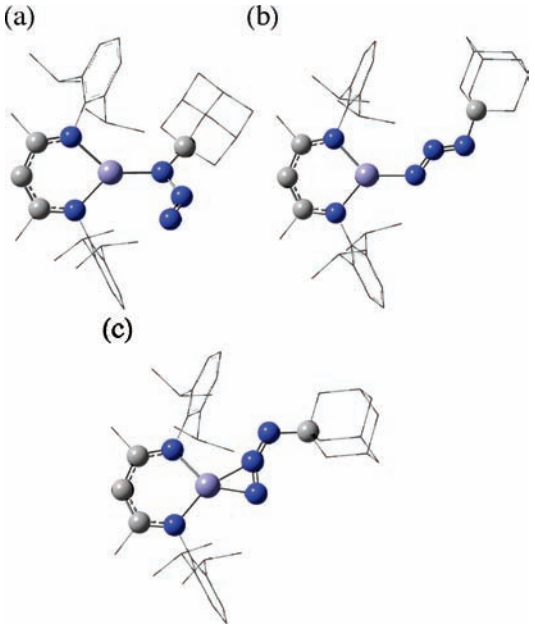

Figure 10. QM/MM optimized geometries of three low energy linkage isomers of $L^{Me}Fe(N_3Ad)$: (a) sextet (κN^1), (b) quartet (κN^3), and (c) quartet η^2. QM atoms are shown as spheres, and MM atoms are shown in wireframe. Hydrogens omitted from figure for clarity.

1.96 Å and the NNN angle is very bent (127°). This is significantly different than in a crystallographically characterized $N_3R\text{-}\kappa N^1$ complex of copper that has a longer Cu−N distance of 2.079(2) Å and a nearly linear NNN angle of 174.5(2)°.[40b] Other crystallographically characterized $N_3R\text{-}\kappa N^1$ complexes also have virtually linear NNN angles (170−178°).[40] The bent NNN angle in particular provided an initial structural hint that the adamantyl azide ligand in

(39) Trautwein, A. X.; Bill, E.; Bominaar, E. L.; Winkler, H. *Struct. Bonding* **1991**, *78*, 1–95.

(40) (a) Albertin, G.; Antoniutti, S.; Baldan, D.; Castro, J.; García-Fontán, S. *Inorg. Chem.* **2008**, *47*, 742–748. (b) Barz, M.; Herdtweck, E.; Theil, W. R. *Angew. Chem., Int. Ed.* **1998**, *37*, 2262–2265. (c) Dias, H. V. R.; Polach, S. A.; Goh, S.-K.; Archibong, E. F.; Marynick, D. S. *Inorg. Chem.* **2000**, *39*, 3894–3901.

Table 3. Calculated Lowest Energy Linkage Isomers of $L^{Me}Fe(N_3Ad)$[a]

isomer	multiplicity	ΔG_{rel}[b]
κN^1	4	0.4
κN^1	6	0.0
κN^3	4	5.0
κN^3	6	16.5
η^2	4	7.1
η^2	6	*c*

[a] Calculated at the B3LYP/6-311+G(d):UFF level of theory. [b] Relative to the lowest energy linkage isomer in kcal/mol (1 atm, 298.15 K). [c] A stationary point corresponding to a sextet η^2 complex was not found at this level of theory; QM/MM geometry optimizations converted to the sextet κN^1 isomer.

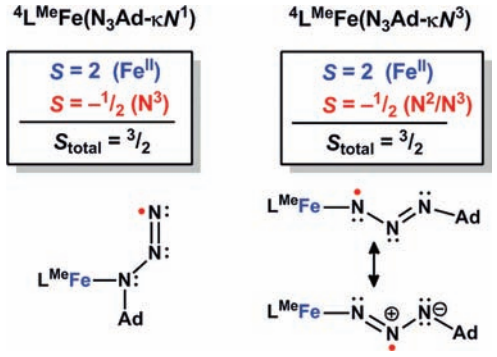

Figure 11. Lewis structures for the two lowest energy isomers of quartet $L^{Me}Fe(N_3Ad)$ implied by the spin density.

these complexes might be reduced to the radical anion. Indeed, separate geometry optimization of the radical anion of N_3Ad leads to a NNN angle (131°) similar to that observed in $^6L^{Me}Fe(N_3Ad\text{-}\kappa N^1)$ (127°). Consistent with this electronic description, the DFT model of $L^{Me}Fe(N_3Ad)$ has substantial spin density on the organoazide ligand. For the lowest energy *sextet*-κN^1 isomer, substantial spin density is found on the terminal (0.75 e^-) and central (0.24 e^-) azide nitrogen atoms, along with ~3.8 e^- on the iron center and the remaining 0.2 e^- on the β-diketiminate nitrogen atoms. For the *quartet* $^4L^{Me}Fe(N_3Ad\text{-}\kappa N^3)$ isomer (ΔG_{rel} = 5.0 kcal/mol, Table 3) there are nearly equal amounts of negative spin density (0.42 e^-) on each of the two nitrogen atoms closest to the iron center, with the remainder almost entirely on the iron center (3.59 e^-). Finally, for the quartet-η^2 isomer the spin density is almost entirely on the iron atom with very little on the organoazide moiety. Figure 11 catalogues the best Lewis structure descriptions of these states derived from the electronic structure analysis.

Elimination of N_2 from $L^{Me}Fe(N_3Ad)$. Two transition states for N_2 elimination were examined, and they differed only by spin state (quartet or sextet). These transition states are close in energy ($\Delta\Delta G^{\ddagger}$ = 1.0 kcal/mol with quartet lower in energy) and are similar in geometry, suggesting facile spin crossover between the quartet and sextet potential energy surfaces. The quartet transition state is depicted in Figure 12, and the sextet transition state is similar. The primary motion from ground state $^6L^{Me}Fe(N_3Ad\text{-}\kappa N^1)$ to the transition state is N^1-N^2 bond lengthening from 1.40 Å to 1.60 Å. The calculated $Fe-N^1$ bond length in the transition state (1.91 Å, Figure 12) is only ~0.05 Å shorter than the corresponding calculated bond length for the ground state, and none of the core bond angles changed by more than ±3°. This similarity of

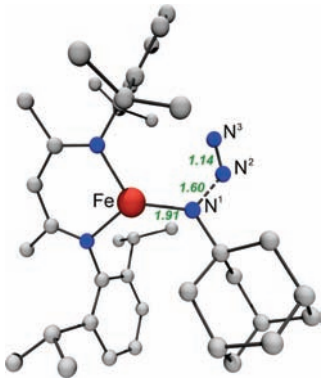

Figure 12. Transition state for N_2 loss from quartet $L^{Me}Fe(N_3Ad\text{-}\kappa N^1)$. Hydrogens omitted from figure for clarity. Relevant distances and angles in the Fe−N−N−N core in the quartet transition state: $Fe-N^1$, 1.91 Å; $Fe-N^3$, 3.31 Å; N^1-N^2, 1.60 Å; N^2-N^3, 1.14 Å; $Fe-N^1-N^2$, 118°; $N^1-N^2-N^3$, 127°. The corresponding sextet transition state is geometrically similar: $Fe-N^1$, 1.94 Å; $Fe-N^3$, 3.19 Å; N^1-N^2, 1.69 Å; N^2-N^3, 1.14 Å; $Fe-N^1-N^2$, 113°; $N^1-N^2-N^3$, 123°.

ground state and transition state geometries in conjunction with the exothermicity of N_2 loss suggests an "early" transition state. The calculated barrier for N_2 loss is $\Delta G^{\ddagger}$ = 12.0 kcal/mol from $^6L^{Me}Fe(N_3Ad\text{-}\kappa N^1)$, where the TS is a quartet. The extrusion of N_2 is exergonic, with ΔG = −43.2 kcal/mol from $^6L^{Me}Fe(N_3Ad\text{-}\kappa N^1)$ to **2** + N_2. Thus, as expected from previous results,[41] expulsion of the stable N_2 and strengthening of the metal−nitrogen linkage provide considerable thermodynamic driving force for imido formation. The overall reaction from 0.5 equiv of $L^{Me}FeNNFeL^{Me}$ to form the corresponding imide (**2**) is exergonic, ΔG = −49.8 kcal/mol.

Pyridine Coordination to Form $L^{Me}Fe(py)_{1,2}$ or $L^{Me}Fe(N_3Ad)(py)$. To explore why coordinating solvents such as pyridine greatly improved the yield of imido complex **2** relative to the hexazene complex **1**, we next endeavored to understand the influence of pyridine coordination on the geometry and relative reaction barriers for N_2 elimination from the Fe-organoazide intermediate. Ligating pyridine to each of the linkage isomers of $L^{Me}Fe(N_3Ad)$ gave adducts with pyridine coordinated in the apical position of a trigonal pyramid whose base is defined by the nitrogens of the β-diketiminate and the ligating nitrogen of the 1-adamantylazide ligand. For the pyridine-coordinated system, the $^4L^{Me}Fe(N_3Ad\text{-}\kappa N^3)$(py) isomer is lowest in energy (Supporting Information, Table S-3 and Figure S-7), which contrasts with "pyridine-free" $L^{Me}Fe(N_3Ad)$, in which $^6L^{Me}Fe(N_3Ad\text{-}\kappa N^1)$ was lowest. Hence, the coordination of pyridine results in a change in preferred AdN_3 coordination mode and spin state. Although it is mildly exothermic, the calculated binding of pyridine is calculated to be overall slightly endergonic (ΔG_{bind} = +4.2 kcal/mol) upon including entropy contributions.[42] Hence, the calculations suggest that binding of pyridine to form $L^{Me}Fe(N_3Ad)$(py) is slightly unfavorable, and that it is expected to be formed only in very small concentrations.

(41) (a) Cundari, T. R.; Pierpont, A. W.; Vaddadi, S. *J. Organomet. Chem.* **2007**, *692*, 4551–4559. (b) Harrold, N. D.; Waterman, R.; Hillhouse, G. L.; Cundari, T. R. *J. Am. Chem. Soc.* **2009**, *131*, 12872–12873.

(42) Note that this binding energy is not the same as the experimental pyridine binding earlier in the paper; Figure 3 describes the binding of pyridine to the imido complex rather than the organoazide complex.

Scheme 4

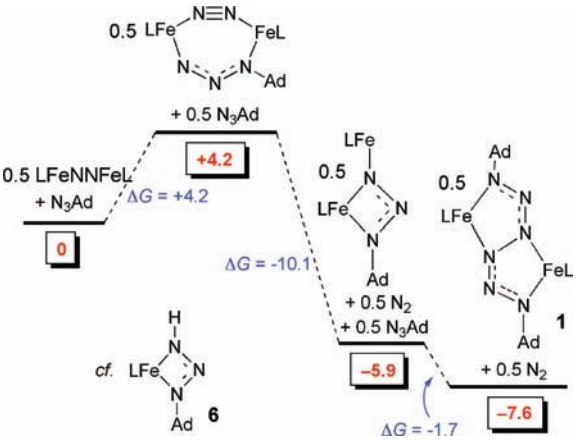

Even though binding pyridine is energetically uphill, we considered the possibility that $L^{Me}Fe(N_3Ad)(py)$ could eliminate N_2 more rapidly than $L^{Me}Fe(N_3Ad)$, explaining the greater yield of **2** in the presence of pyridine discussed above. The calculated barrier to N_2 elimination from $^4L^{Me}Fe(N_3Ad\text{-}\kappa N^3)(py)$ (the lowest energy linkage isomer) is calculated to be $\Delta G^{\ddagger} = +9.8$ kcal/mol.[43] Thus, the total barrier for N_2 elimination from $^6L^{Me}Fe(N_3Ad\text{-}\kappa N^1)$ through a pathway involving pyridine coordination is $\Delta G^{\ddagger} = +14$ kcal/mol, which is similar to that without pyridine ($\Delta G^{\ddagger} = +12$ kcal/mol). Therefore, there is no compelling computational evidence that coordination of a donor to $L^{Me}Fe(N_3Ad)$ facilitates N_2 loss.

We also evaluated the energetics of $L^{Me}Fe(py)$ and $L^{Me}Fe(py)_2$, the potential products of AdN_3 *displacement* by pyridine. Both $L^{Me}Fe(py)$ and $L^{Me}Fe(py)_2$ are 11−12 kcal/mol uphill from $L^{Me}Fe(N_3Ad)$ (see Supporting Information, Figure S-9), suggesting that these species are unlikely to be formed if an organoazide is present.

Diiron Intermediates Leading to Hexazene 1. Instead of forming a 1:1 Fe/organoazide intermediate, another possibility is that N_3Ad reacts with the iron(I) dimer $L^{Me}FeNNFeL^{Me}$ to give a *diiron*−organoazide intermediate. The possible intermediates $L^{Me}Fe(\mu\text{-}N_2\text{-}1\kappa\text{-}N^1\text{:}2\kappa\text{-}N^2)(\mu\text{-}N_3Ad\text{-}1\kappa\text{-}N^1\text{:}2\kappa\text{-}N^3)FeL^{Me}$ and $L^{Me}Fe(\mu\text{-}N_3Ad\text{-}1\kappa^2\text{-}N^1,N^3\text{:}2\kappa\text{-}N^3)FeL^{Me}$ (shown in Scheme 4) were thus investigated; energies below are calculated as 0.5 equivalent of dimer to maintain consistent energy accounting relative to the monomeric iron complexes in other mechanisms. The formation of $L^{Me}Fe(\mu\text{-}N_2\text{-}1\kappa\text{-}N^1\text{:}2\kappa\text{-}N^2)(\mu\text{-}N_3Ad\text{-}1\kappa\text{-}N^1\text{:}2\kappa\text{-}N^3)FeL^{Me}$ from $L^{Me}FeNNFeL^{Me}$ and N_3Ad is mildly endergonic ($\Delta G = +4.2$ kcal/mol), and loss of N_2 from this species to give $L^{Me}Fe(\mu\text{-}N_3Ad\text{-}1\kappa^2\text{-}N^1,N^3\text{:}2\kappa\text{-}N^3)FeL^{Me}$ is exergonic ($\Delta G = -10.1$ kcal/mol). Consistent with a formulation as a diiron(II) complex and a dianionic AdN_3^{2-} ligand, the spin density in $L^{Me}Fe(\mu\text{-}N_3Ad\text{-}1\kappa^2\text{-}N^1,N^3\text{:}2\kappa\text{-}N^3)FeL^{Me}$ is primarily on the iron atoms.

Though bimetallic complexes with organoazides in the $\mu\text{-}1\kappa^2\text{-}N^1,N^3\text{:}2\kappa\text{-}N^3$ mode are rare, two examples in the literature with crystallographic characterization support the feasibility of dianionic bridging organoazides with the same coordination. The dialuminum complex $((Me_3Si)_2HC)_2Al(\mu\text{-}N_3SiMe_3\text{-}1\kappa^2\text{-}N^1,N^3\text{:}2\kappa\text{-}N^3)Al(CH(SiMe_3)_2)_2$ has been characterized,[44] and assuming the aluminum(III) oxidation state suggests that the bridge is dianionic, as postulated in the calculated diiron intermediate. More recently, the bulky terphenyl group R* (R* = 2,6-bis(2,6-diisopropylphenyl)-phenyl) was used to support $R^*Cr(\mu\text{-}N_3Ad\text{-}1\kappa^2\text{-}N^1,N^3\text{:}2\kappa\text{-}N^3)CrR^*$, in which the bridging 1-adamantylazide is again dianionic.[45] The core angles and distances in the crystal structures of these molecules are similar to those in the computational model of the diiron intermediate (see Supporting Information, Figure S-4). The four-membered FeNNN ring of $L^{Me}Fe(\mu\text{-}N_3Ad\text{-}1\kappa^2\text{-}N^1,N^3\text{:}2\kappa\text{-}N^3)FeL^{Me}$ also bears a striking resemblance to that in the previously characterized iron(II) triazenido complex $L^{tBu}Fe(AdNNNH\text{-}\kappa^2\text{-}N^1,N^3)$ (**6**, see diagram in Scheme 4).[24d]

During attempts to crystallize **4** (with the bulkier L^{tBu} ligand), we fortuitously obtained a crystal structure (Supporting Information, Figure S-3) of $L^{tBu}Fe(\mu\text{-}N_3Ad)FeL^{tBu}$, which has the core structure of the second hypothetical intermediate.[46] Although we have not been able to generate this species reproducibly for further characterization, and the crystal was of poor quality, the preliminary observation of a species with this connectivity supports the feasibility of bimolecular organoazide-bridged intermediates in the L^{Me} system.

The computations indicate that the diiron organoazide complex is capable of leading to the final hexazene product (**1**). Addition of an additional 0.5 N_3Ad to 0.5 $L^{Me}Fe(\mu\text{-}N_3Ad)FeL^{Me}$ to give 0.5 equiv of **1** is slightly exergonic, $\Delta G = -1.7$ kcal/mol. The overall reaction from 0.5 $L^{Me}FeNNFeL^{Me}$ to 0.5 equiv **1** is exergonic as well, $\Delta G = -7.6$ kcal/mol. The potential energy surface showing the relative energies of these species is shown in Scheme 4.

Discussion

In the synthesis of late transition metal imido complexes, organoazides are an excellent source of the "nitrene" fragment because N_2 is the only byproduct, and because organoazides are generally easy to synthesize. In this work, we used the addition of 1-adamantyl azide to an iron(I) synthon to create a well-characterized iron(III) imido complex with a trigonal planar geometry. Similar reactions have been used to generate isolable three-coordinate cobalt(III) and nickel(III) imido complexes of a smaller β-diketiminate ligand, though studies on the mechanism of these interesting reactions have not yet been reported.[16c,18] Our computational and synthetic studies suggest that interaction of diketiminate-iron(I) species with organoazide forms an iron-organoazide complex $L^{Me}Fe(N_3Ad)$.

Comparison of $L^{Me}Fe(N_3Ad)$ to Literature Organoazide Complexes. Vaddadi et al. have complemented the experimental studies of Hillhouse[17b] by investigating the mechanism of decomposition of coordinated organoazides via DFT calculations on (dhpe)Ni(N_3Me) and (dhpe)Ni(N_3Ns) (Ns = *p*-nitrophenylsulfonyl) model

(43) A potential energy surface showing the relative energies of $L^{Me}Fe(N_3Ad)$, $L^{Me}Fe(N_3Ad)(py)$, and the N_2 elimination transition states is given in Supporting Information, Figure S-7.

(44) Uhl, W.; Gerding, R.; Pohl, S.; Saak, W. *Chem. Ber.* **1995**, *128*, 81–85.

(45) Ni, C.; Ellis, B. D.; Long, G. J.; Power, P. P. *Chem. Commun.* **2009**, 2332–2334.

(46) This structure resulted from an unsuccessful attempt to isolate **4**. Concentrated pentane solutions of $L^{tBu}FeNNFeL^{tBu}$ and N_3Ad (1:2) were added together at −45 °C and kept at −45 °C overnight, resulting in the deposition of an amorphous red-brown solid and a very small quantity of well-formed orange crystals of $L^{tBu}Fe(\mu\text{-}N_3Ad)FeL^{tBu}$.

systems, dhpe = $H_2PCH_2CH_2PH_2$.[47] Morello and Cundari have extended this computational research to the study of the decomposition of prototypical nitrene transfer reagents used in organic synthesis, such as tosyl azides, Chloramine-T, and iodonium imides.[22b] For a d^{10} Cu^I−scorpionate complex, a κN^3 linkage isomer has been structurally characterized by Dias and co-workers (Figure 9a).[40c] In this complex, the CuNN and NNN angles are observed to be nearly linear by X-ray crystallography, suggesting a neutral organoazide ligand. Most other examples of κN^3 coordination also have essentially linear NNN angles,[40] and computations[40c] support the assignment of a neutral N_3R ligand. These late transition metal complexes are distinct from the κN^3 organoazides ligated to complexes of earlier transition metals, such as the tantalum(V) and vanadium(V) organoazide complexes reported by the groups of Bergman[20a,b] and Cummins,[20c] respectively. In these complexes, the short M−N bond and bent NNN and NNC angles are suggestive of a prevailing diazenylimido ($L_nM{=}N{-}N{=}N{-}R$) bonding description with a dianionic ligand.

In this work, we describe computations that support the best description of $L^{Me}Fe(N_3Ad)$ with a form of coordinated organoazide that is different than those described above. In the complex, the organoazide is best described as a one-electron reduced $N_3Ad^{\bullet-}$ ligand, which is coordinated through the internal nitrogen atom (κN^1). The assignment as a radical anion ligand is based on the bond lengths and N−N−N bond angle that are very similar to those calculated for the free $N_3Ad^{\bullet-}$ anion, and by the observation of roughly one electron of spin density on the coordinated organoazide. This assignment implies that the iron is in the iron(II) oxidation state. High-spin iron(II) can magnetically couple with the organoazide radical to give overall quartet or sextet states, and the nearly identical energies calculated for these two states suggests a very small value of the exchange coupling J despite the short distance between the two paramagnetic subsites. Because the species so rapidly reacts to give other products, we were not able to evaluate its properties experimentally except through the distribution of products derived therefrom (see below).

The one-electron reduction of a coordinated ligand by the "$L^{Me}Fe$" fragment has ample precedent. In the tetrazene complex $L^{Me}Fe(AdNNNNAd\text{-}\kappa^2N^1,N^4)$ (**5**), magnetic and spectroscopic studies showed that the tetrazene ligand exists as a radical anion coordinated to iron(II).[48] Similarly, a combination of spectroscopic and computational studies showed that $L^{Me}Fe$(alkyne) complexes have one electron localized in a π^* orbital of the alkyne fragment.[24b] In bimetallic examples, the dinitrogen complex $L^{Me}FeNNFeL^{Me}$ is best described as a diiron(II) complex of the N_2^{2-} anion, and reaction of the iron(I) fragment with acetophenone gives pinacol coupling.[23b] In an analogy to the radical organoazide ion postulated here, Peters recently reported an iron complex with $N_3Ad\text{-}\kappa N^3$ coordination and an NNN angle of 147(4)°, for which DFT computations showed a spin density of 0.77 e^- on the organoazide, suggesting the assignment of a monoanionic N_3Ad ligand.[49]

Another useful comparison is to complexes (dtbpe)Ni(η^2-N_3R) (dtbpe = bis(di-*tert*-butylphosphino)ethane; R = Ad, Mes; see Figure 9c), which were structurally characterized and spontaneously convert into the stable imido complexes (dtbpe)Ni=NR.[17b] The crystal structures of (dtbpe)Ni(N_3R) each show the η^2-N_3R isomer, in contrast to $L^{Me}Fe(N_3Ad)$, in which the κN^1 isomer has the lowest energy by DFT. It is interesting to note the difference in preferred coordination mode, despite both (dbtpe)Ni(N_3R) and $L^{Me}Fe(N_3Ad)$ utilizing bulky bidentate supporting ligands.

Mechanism of Forming Hexazene Products. The hexazene complex **1** is conceptually derived from reductive coupling of two N_3Ad molecules to give an $Ad_2N_6^{2-}$ bridge.[25] Given the computational results that indicate $L^{Me}Fe(N_3Ad)$ has substantial unpaired spin density on the organoazide ligand when coordinated η^1, we initially considered that formation of the diiron(II) hexazene complex could result from simple radical dimerization of two molecules of $L^{Me}Fe(N_3Ad^{\bullet})$. However, QM/MM computations presented above indicate that there is not a significant thermodynamic driving force for this dimerization (ΔG = −0.6 kcal/mol per Fe), especially in comparison to the formation of the imido product **2** (ΔG = −42.8 kcal/mol) in which the barrier height is calculated to be low ($\Delta G^{\ddagger}$ = 12 kcal/mol). Although the dimerization of $L^{Me}Fe(N_3Ad)$ molecules may be a contributing mechanism, the mechanism involving diiron intermediates (Scheme 4) is also reasonable, and more easily explains the solvent dependence of the product distribution (see below). The feasibility of bimetallic intermediates of the type $\{LFe\}_2(\mu\text{-}N_3Ad)$ is shown by the fortuitous crystallization of $L^{tBu}Fe(\mu\text{-}N_3Ad)FeL^{tBu}$, although rational synthesis and characterization of this compound has not been achieved at this time.

Why is a Coordinating Solvent Needed during the Synthesis of 2? We now turn our attention to the solvent effect on the outcome of the reaction $L^{Me}FeNNFeL^{Me}$ + 2 N_3Ad. The most coordinating solvents (THF, pyridine, or arenes[50]) gave the highest yields of imido product **2** and lowest conversion to hexazene **1** (Table 1). The dominance of solvent coordination (rather than polarity) is most convincingly demonstrated by the difference between the outcomes of reactions performed in THF and 2,5-dimethyl-THF. This pair of solvents has previously been used to distinguish between rate effects of polarity (the solvents have similar polarities) versus coordination (dimethyl-THF is sterically prevented from coordinating).[51] In THF, the yield of **2** is 80% (9:1 imido/hexazene), while in the much less coordinating 2,5-dimethyl-THF the yield of **2** is only 28% (1:2 imido/hexazene). Likewise, $PhCF_3$ gives more imido complex (59% yield, 3:1 imido/hexazene) than toluene (41% yield, 1:1 imido/hexazene) because it is a better π-acceptor, and should bind more strongly to iron(I).[24c,50]

(47) Cundari, T. R.; Vaddadi, S. *THEOCHEM* **2006**, *801*, 47–53.
(48) Cowley, R. E.; Bill, E.; Neese, F.; Brennessel, W. W.; Holland, P. L. *Inorg. Chem.* **2009**, *48*, 4828–4836.
(49) Mankad, N. P.; Müller, P.; Peters, J. C. *J. Am. Chem. Soc.* **2010**, *132*, 4083–4085.
(50) Arenes are competitive ligands for iron(I) because of the strength of backbonding from Fe to π^* orbitals of the arene fragment. References 24b and 24c contain examples of diketiminate-supported iron(I)-arene complexes.
(51) Wax, M. J.; Bergman, R. G. *J. Am. Chem. Soc.* **1981**, *103*, 7028–7030.

Scheme 5

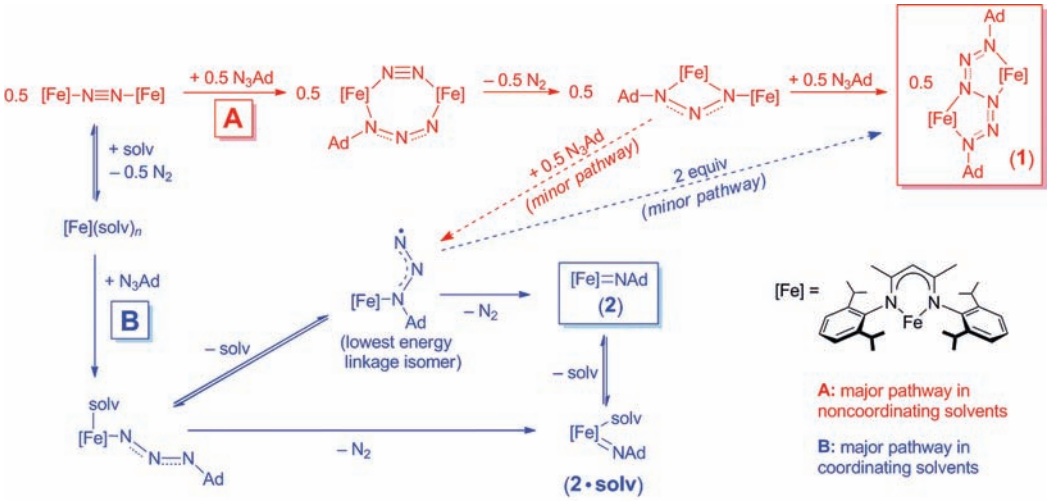

Hypothesis 1: Donor Solvents Compete with Organoazide for Coordination. We first considered an explanation in which donor solvents displace organoazide from $L^{Me}Fe(N_3Ad)$, decreasing the concentration of this key intermediate. Because conversion of $L^{Me}Fe(N_3Ad)$ to **1** is bimolecular and to **2** is unimolecular, any decrease in the concentration of $L^{Me}Fe(N_3Ad)$ from a donor solvent would disfavor coupling to form **1**. This is consistent with the production of **2** in donor solvents and **1** in other solvents. To test this idea, we used computations to gauge the influence of pyridine, one of the most effective donors, on potential intermediate species. However, the QM/MM calculations show that *pyridine is not capable of displacing organoazide from* $L^{Me}Fe(N_3Ad)$; the exchange is calculated to be uphill by $\Delta G = +12$ kcal/mol. The displacement of organoazide should be even less favorable for weaker donors such as THF. Therefore, the computations cast significant doubt on the verity of this hypothesis.

Hypothesis 2: Lewis Bases Catalyze Imido Formation. In a second potential explanation, we hypothesized that donor solvents catalyze N_2 loss to form **2** by binding to the $L^{Me}Fe(N_3Ad)$ intermediate and transiently forming the more crowded complex $L^{Me}Fe(N_3Ad)$(solvent). If this binding were to lower the barrier to N_2 elimination, a donor solvent would accelerate imido formation relative to hexazene formation. However, computations indicated that addition of pyridine does not lower the barrier to N_2 elimination ($\Delta G^{\ddagger} = +12$ kcal/mol from $L^{Me}Fe(N_3Ad)$, and $\Delta G^{\ddagger} = +14$ kcal/mol from $L^{Me}Fe(N_3Ad)$(py)). Alternatively, the rate of dimerization of $L^{Me}Fe(N_3Ad)$(solvent) giving hexazene **1** should be slower than the dimerization of $L^{Me}Fe(N_3Ad)$ since the terminal N is less exposed in the solvent-coordinated complex. However, $L^{Me}Fe(N_3Ad)$(py) is computed to be +4.2 kcal/mol higher in energy than $L^{Me}Fe(N_3Ad)$, and thus the concentration of $L^{Me}Fe(N_3Ad)$(py) would not be significant enough to slow down the rate of hexazene formation. Thus, neither displacement of N_3Ad by solvent forming $L^{Me}Fe$(solvent) nor coordination of pyridine forming $L^{Me}Fe(N_3Ad)$(solvent) adequately explains the observed solvent effect.

Hypothesis 3: Separate Pathways to Hexazene and Imido. Elimination of the two aforementioned explanations leaves the possibility that hexazene and imido products proceed through different mechanisms: one mechanism from the bridging N_2 complex $L^{Me}FeNNFeL^{Me}$ that leads to hexazene **1** in the absence of a donor solvent, and another mechanism from the mononuclear $L^{Me}Fe$(solvent) species that leads to imido **2**. This explanation is fully consistent with the computational results. First, AdN_3 is capable of displacing donor solvents and N_2 because it binds strongly. Second, computations show that dinuclear $L^{Me}FeNNFeL^{Me}$ can access an energetically favorable bimetallic reaction with AdN_3 that leads directly to hexazene **1**. The bimetallic mechanism proceeds without formation of $L^{Me}Fe(N_3Ad)$ (Scheme 3), and requires no coordinating solvent. Coordination of solvent would partially or completely displace N_2 in $L^{Me}FeNNFeL^{Me}$, eliminating the bimetallic mechanism that gives **1**, and opening up the monometallic mechanism through $L^{Me}Fe(N_3Ad)$ to **2**.

Overall Mechanistic Picture of the Reaction of Adamantyl Azide with Low-Valent Iron. The most consistent mechanistic picture relating **1**, **2**, **2·solvent**, and $L^{Me}Fe(N_3Ad)$ is given in Scheme 5, which starts in the upper left with a mixture of $L^{Me}FeNNFeL^{Me}$ and $L^{Me}Fe(solvent)_n$. Adamantyl azide either displaces the N_2 ligand in $L^{Me}FeNNFeL^{Me}$, forming $L^{Me}Fe(\mu\text{-}N_3Ad)FeL^{Me}$ (pathway **A**), or displaces solvent in $L^{Me}Fe(solvent)_n$, forming $L^{Me}Fe(N_3Ad)$ (pathway **B**). Neither iron−organoazide intermediate is observed during the reaction. *In noncoordinating solvents* such as pentane, iron is only present as the bimetallic N_2 complex, which primarily proceeds along pathway **A** to give the diiron organoazide species $L^{Me}Fe(\mu\text{-}N_3Ad)FeL^{Me}$, and leads to the diiron(II) hexazene product **1** upon addition of the second N_3Ad molecule. A small amount of **2** is also formed through crossover to pathway **B**, which is accessed if any of the dimers are cleaved (the blue "minor pathway" in Scheme 5). *In coordinating solvents* such as THF or pyridine, the diiron-N_2 complex is in equilibrium with the solvated iron(I) compound $L^{Me}Fe(solvent)_n$, and the exergonic addition of N_3Ad gives discrete monomeric $L^{Me}Fe(N_3Ad)$ or $L^{Me}Fe(N_3Ad)$(solvent) along pathway **B**, leading to **2** as the major product. Formation of small amounts of **1** could occur through radical coupling of $L^{Me}Fe(N_3Ad)$ (marked "minor pathway" in Scheme 5), or from conversion of $L^{Me}Fe(N_3Ad)$ to $L^{Me}Fe(\mu\text{-}N_3Ad)FeL^{Me}$.

Once formed, complex **2** also reversibly coordinates pyridines such as ^{t}Bupy, forming small amounts of **2**·^{t}**Bupy**. This is important, since four-coordinate imido complex **2**·^{t}**Bupy** is much more reactive to sources of H$^\bullet$ than **2**.[28,33] The fast reaction of **2**·^{t}**Bupy** with 1,4-cyclohexadiene (CHD) to afford the amido species L^{Me}Fe(NHAd)(^{t}Bupy) (**3**·^{t}**Bupy**)[28] is a convenient test of whether **1** can transiently form **2** in solution. Complex **1** did not form detectable quantities of **3**·^{t}**Bupy** by ^{1}H NMR spectroscopy when heated to 80 °C in the presence of 100 equiv of 1,4-cyclohexadiene and 10 equiv of ^{t}Bupy. Therefore, the formation of **1** is irreversible and cannot access the imido complex **2**.

The most synthetically useful solvent for the preparation of **2** has proven to be THF, since it is coordinating enough to steer the product distribution mostly away from hexazene **1**, but does not coordinate to the imido product. Although small amounts of ^{t}Bupy also gave a desirable imido/hexazene ratio (7:1), the presence of pyridine catalyzes the decomposition of **2** by "turning on" hydrogen atom abstraction (HAA) pathways.[28,33]

Implications For the Larger L^{tBu} System. The mechanistic picture relating **1**, **2**, and L^{Me}Fe(N_3Ad) in Scheme 5 is explicit only for the L^{Me} system. Using L^{tBu} as the supporting ligand leads to a good yield of imido complex **4** even in pentane, and thus coordinating solvents are not necessary to avoid hexazene formation at room temperature. This observation can be accommodated within the mechanistic picture in Scheme 5 using different relative rates of the individual steps. We speculate that in the L^{tBu}Fe system, the reaction begins along the diiron pathway **A** (as for the L^{Me} system in pentane), giving L^{tBu}Fe(μ-N_3Ad)FeL^{tBu} (see above) as a key intermediate. Since the added steric bulk of the L^{tBu} ligand destabilizes the diiron intermediates at the top of Scheme 5, the fragmentation to L^{tBu}Fe(N_3Ad) (red "minor pathway") would be more rapid, and the attack of a second azide (giving hexazene) would be slower than in the L^{Me} system. This corresponds to crossover from the bimetallic manifold **A** to the monoiron manifold **B** (i.e., the red downward "minor pathway" arrow in Scheme 5 becomes the major pathway). Though the inability to characterize intermediates prevents us from further supporting this mechanistic scheme for the L^{tBu} system, it is important that a single mechanistic scheme can rationalize all the trends in the reaction outcomes for both L^{Me} and L^{tBu} complexes.

Properties of Imidoiron(III) Complex 2. Though **2** is only metastable (solids or solutions must be kept at reduced temperature to have lifetimes of more than a few hours), it has been crystallized and characterized through several methods. Crystallographic data show a short iron−nitrogen bond similar to those in other iron(III)-imido complexes (further analysis below). These data are supported by X-ray absorption studies, which also show similar features in the uncrystallized L^{tBu}Fe-NAd (**4**). Therefore, the spectroscopic evidence gleaned from solutions of **2**·^{t}**Bupy**[28] and **4**[34] in previous communications are now supported by compelling structural data.

The greater purity of **2** has enabled the use of additional physical techniques. For example, ^{1}H NMR spectra show that **2** reversibly binds pyridine but not THF. Note that the ^{1}H NMR spectra of **2** are surprisingly narrow for an iron(III) complex. This is the result of the intermediate-spin (S = 3/2) ground state of the iron(III) ion, which has fairly low-lying excited states that enable rapid electronic relaxation and hence slow nuclear relaxation.[52] The quartet ground state was inferred from X-band EPR spectra of mixtures containing **2** in previous studies,[28] and is now supported by magnetic susceptibility studies on crystalline **2**, as well as X-band EPR spectra of purified **2**.

Structural Trends in Fe, Co, and Ni Imido Complexes. As a result of the recent successes in stabilizing imido complexes of the late first-row transition metals,[12−18] there now exist enough structurally characterized examples (Supporting Information, Table S-6) to begin to evaluate trends.

The first notable feature is that the isolable Fe, Co, and Ni imido complexes always have coordination numbers of three or four.[53] This generalization can be rationalized by examining the ligand field splitting, which shows that trigonal-planar and tetrahedral geometries (as well as square-planar if not low-spin) lead to incomplete occupation of the d-orbitals that have the correct symmetry for π-bonding with the imido group.[12,13,16,18,19,28] The interaction of empty (or partially empty) d orbitals with p-orbitals of sp-hybridized nitrogen in the imido ligand leads to π-bonding. In low-spin octahedral and square-planar geometries, the appropriate d orbitals are filled, and there can be no stabilizing π-interactions.[3]

Further details can be gleaned from a search of the Cambridge Crystallographic Database. Figure 13 shows a scatter plot of M=N bond length versus M=N−C bond angle for all known structurally characterized examples of terminal imido complexes of Fe, Co, and Ni, organized by both metal and coordination geometry.[54]

Although there is significant scatter in the data, a few points are worth mentioning. First, there is little correlation between M=N bond length and M=N−C bond angle, an observation which has also been noted in early transition metal imido complexes.[55] Second, neither the average M=N bond length (Fe, 1.64(3) Å (n = 19); Co, 1.65(2) Å (n = 9); Ni, 1.69(2) Å (n = 4)) nor the M=N−C bond angle (Fe, 172(7)°; Co, 173(6)°; Ni, 168(8)°) are dependent on the identity of the metal. Third, Figure 13b does suggest that the bond metrics are dependent on the *coordination geometry* of the metal. Thus, tetrahedral imido complexes have a more linear M=N−C angle (176(3)°, n = 21) than trigonal (166(7)°, n = 9) imido complexes (p = 0.0017), and also have a more linear angle than square-planar (162(5)°, n = 2) imido complexes (p = 0.11). Tetrahedral complexes can give two M=N π-bonds (metal−nitrogen triple bond), but partial occupation of M=N π^* orbitals in the planar complexes gives less metal−nitrogen π bonding.[12,13,16,18,19] It is reasonable that the M=N−C angle would be the metrical

(52) La Mar, G. N.; Horrocks, W. D.; Holm, R. H. *NMR of Paramagnetic Molecules*, Academic Press, New York, 1973.

(53) Treating the six-electron donors Cp* or arene as three "electron pairs" is necessary to account for the imido complexes in refs 9−11. See also: Glueck, D. S.; Green, J. C.; Michelman, R. I.; Wright, I. N. *Organometallics* **1992**, *11*, 4221–4225.

(54) Included in the analysis are all the examples included up to the Feb 2010 update of the CSD (v. 5.31), the structure reported in reference 16f, and compound **2** in this work. See SI for details.

(55) Cundari, T. R.; Russo, M. *J. Chem. Inf. Comput. Sci.* **2001**, *41*, 281–287.

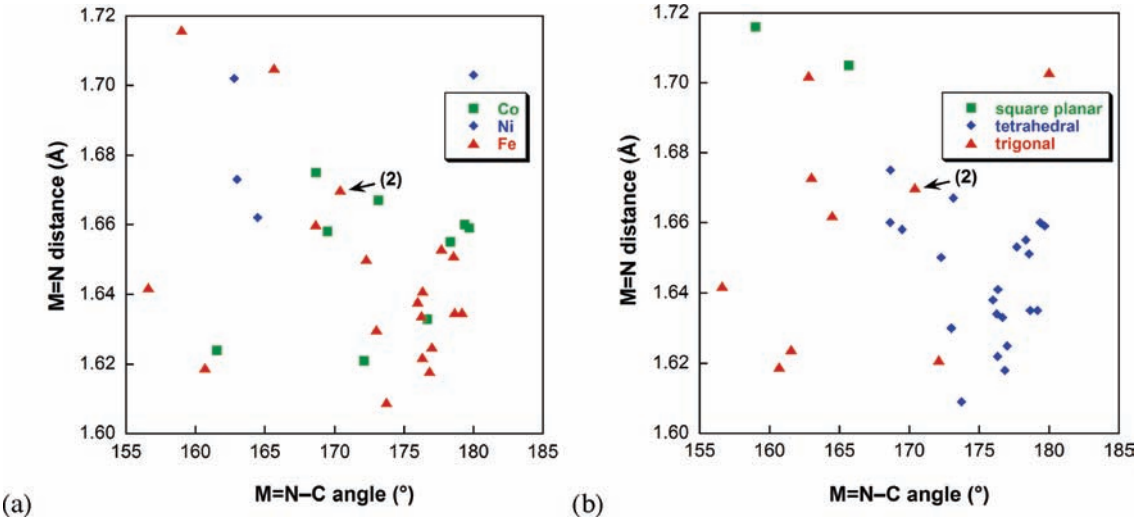

Figure 13. Correlation of M=N bond lengths with M=N−C bond angle in literature Fe, Co, Ni complexes with terminal imido ligands, organized by (a) metal and (b) coordination geometry. For crystal structures with multiple molecules in the asymmetric unit, the average bond parameters are used. The data are tabulated in Supporting Information, Table S-6. Compound **2** in this work is indicated with the arrow.

parameter that is most responsive to this effect because computational studies have shown that bending the imido ligand at nitrogen is "soft" (i.e., not energetically costly).[2,55]

It is interesting to note that the most reactive Fe, Co, and Ni imido complexes feature a trigonal or square-planar ligand field, the same geometry that gives somewhat more acute M=N−C angles. The only catalytic reactions that have been reported using isolable Fe, Co, or Ni imido complexes are organoazide hydrogenation with a square-planar Fe(III) imido complex,[13c] and formation of carbodiimides and isocyanates by trigonally coordinated iron[34] and nickel[56] imido complexes. Trigonal copper-imido/copper-nitrene complexes have been implicated as the active intermediates in catalytic C−H amination reactions and catalytic diazene formation reported by Warren and co-workers.[7ff,57] Therefore, the M=N−C bending seen in planar imido complexes may correlate with an increase in their reactivity. On the other hand, Peters recently showed catalytic diazene formation through a spectroscopically characterized, presumably trigonal-bipyramidal, imidoiron(III) species.[49] Also, Gallo recently reported porphyrin-cobalt complexes that catalyze amination.[58] Thus, putative higher-coordinate imido species can be reactive as well.

Conclusions

The reaction of adamantyl azide with the iron(I) precursors $L^RFeNNFeL^R$ (L^R = bulky β-diketiminate ligand) gives several unusual results. DFT analysis of the putative metal-organoazide complex $L^{Me}Fe(N_3Ad)$ shows that $L^{Me}Fe^{II}(N_3Ad^{\bullet-})$ is the best valence description. The bending of the NNN unit in the organoazide complex leads to facile N_2 loss and formation of a trigonal iron(III) imido complex $L^{Me}Fe{=}NAd$ (**2**).

Though reactive and unstable, this imidoiron complex has been characterized in great detail. X-ray absorption and diffraction experiments demonstrate that the Fe=N bond is short, in the range of a double bond. Solid-state magnetic susceptibility and solution EPR spectroscopy of **2** show that it has an isolated quartet ground state, consistent with computational studies.[28] Comparison to literature iron-imido species suggests that a planar geometry at the metal, as found here, may be responsible for the bending of the M=N−C angle and heightened reactivity.

The reaction to form $L^{Me}FeNAd$ is complicated by formation of the diiron hexazene complex $\{L^{Me}Fe\}_2(N_6Ad_2)$ (**1**). The ratio of imido and hexazene products is solvent dependent, with coordinating solvents (THF, ^{t}Bupy) steering the reaction toward imido formation. Computational studies led to a mechanistic scheme in which donor solvents separate the bimetallic complex $L^{Me}FeNNFeL^{Me}$ into monometallic units, which are less likely to undergo a bimetallic reaction pathway toward hexazene. We have shown that the traditional synthesis of imidometal complexes from organoazide and a low-valent metal can be hampered by unexpected side reactions such as organoazide coupling, and that making subtle adjustments to the reaction (THF vs pentane solvent) can greatly influence the outcome. These insights contribute to the burgeoning field of late transition metal imido complexes, and help to shed light on the formation and properties of these catalytically active species.

Experimental Section

General Considerations. All manipulations were performed under a nitrogen atmosphere in an MBraun glovebox maintained at or below 1 ppm of O_2 and H_2O. 1-Adamantyl azide was purchased from Aldrich and crystallized twice from pentane prior to use. 1,4-Cyclohexadiene was purchased from Aldrich, vacuum distilled from calcium chloride, and stored over activated 3 Å molecular sieves. 4-*tert*-Butylpyridine was purchased from Aldrich, vacuum distilled from CaH_2, and stored over activated 3 Å molecular sieves. The compounds $[L^{Me}FeCl]_2$,[31] $L^{Me}FeNNFeL^{Me}$,[23] and $L^{tBu}Fe{=}NAd$[34] were prepared as previously described. Pentane, diethyl ether, THF, and toluene were purified by passage through activated alumina and Q5 columns from Glass Contour Co. (Laguna Beach, CA). Benzene-d_6 was

(56) Laskowski, C. A.; Hillhouse, G. L. *Organometallics* **2009**, *28*, 6114–6120.
(57) For a theoretical study on these Cu-nitrene complexes, see: Cundari, T. R.; Dinescu, A.; Kazi, A. B. *Inorg. Chem.* **2008**, *47*, 10067–10072.
(58) Fantauzzi, S.; Caselli, A.; Gallo, E. *Dalton Trans.* **2009**, 5434–5443.

dried over flame-activated alumina. Toluene-d_8 and THF-d_8 were vacuum transferred from purple sodium benzophenone ketyl solutions. THF and THF-d_8 were stored over Na metal. Before use, an aliquot of each solvent was tested with a drop of sodium benzophenone ketyl in THF. Celite was dried at 250 °C overnight under vacuum. All glassware was dried overnight in a 150 °C oven. NMR data were collected on either a Bruker Avance 400 or Bruker Avance 500 spectrometer and spectra are referenced to residual C_6D_5H (δ 7.16 ppm), C_4D_7HO (δ 3.58 ppm), or C_7D_7H (δ 2.08 ppm). The NMR probe temperature was calibrated using either ethylene glycol or methanol.[59] IR data were recorded on a Shimadzu 8400S spectrometer using KBr. UV−vis spectra were recorded on a Cary 50 spectrometer using screw-cap or Schlenk-adapted cuvettes. Elemental analysis was determined by Columbia Analytical Services, Tucson, AZ. Room temperature solution magnetic susceptibilities were determined by the Evans method.[60]

L^{Me}FeNAd (2). A 20 mL scintillation vial was loaded with $L^{Me}FeNNFeL^{Me}$ (298 mg, 0.306 mmol) and THF (15 mL) to give a royal purple solution. A solution of N_3Ad (108 mg, 0.611 mmol) in THF (2 mL) was added dropwise causing effervescence and a color change to dark yellow-brown. The reaction was stirred for 15 min, and the volatile materials were removed under vacuum. The residue was redissolved in pentane (~8 mL), the solution was filtered through Celite, and the volatile materials were removed under vacuum. The residue was dissolved in a minimum amount of pentane (~4 mL) and cooled to −45 °C, giving crystalline **2** in two crops (231 mg, 61%). ^{1}H NMR (500 MHz, C_6D_6): δ 84.4 (6H, Ad-H$_\alpha$), 53.4 (1H, α-CH), 37.4 (3H, Ad-H$_\beta$ or Ad-H$_\gamma$), 34.5 (3H, Ad-H$_\beta$ or Ad-H$_\gamma$), 24.2 (3H, Ad-H$_\beta$ or Ad-H$_\gamma$), −10.1 (12H, CH(CH_3)$_2$), −14.8 (4H, *m*-Ar or C*H*(CH$_3$)$_2$), −24.0 (6H, Me), −28.1 (2H, *p*-Ar), −58.4 (12H, CH(CH_3)$_2$), −74.6 (4H, *m*-Ar or C*H*(CH$_3$)$_2$) ppm. IR: 3056 (w), 2958 (s), 2920 (s), 2900 (s), 2865 (m), 2845 (m), 1522 (s), 1458 (m), 1437 (m), 1384 (s), 1319 (s), 1260 (w), 1177 (w), 1100 (w), 1056 (w), 1027 (w), 936 (w), 797 (m), 757 (m) cm^{-1}. UV/vis (pentane): 323 (19 mM^{-1} cm^{-1}), 410 (4.0 mM^{-1} cm^{-1}), 480 (sh, ~2 mM^{-1} cm^{-1}), 580 (sh, ~0.4 mM^{-1} cm^{-1}) nm. μ_{eff} (C_6D_6, 25 °C): 4.4 ± 0.3 μ_B.

L^{Me}FeNHAd (3). Method A (from L^{Me}FeNAd (1) and 1,4-Cyclohexadiene). A J-Young NMR tube was loaded with **2** (11.7 mg, 18.8 μmol) and C_6D_6 (0.6 mL). 1,4-Cyclohexadiene (17.8 μL, 188 μmol) was added, and the reaction was monitored by ^{1}H NMR spectroscopy at 23 °C. After 90 min no **2** remained and L^{Me}FeNHAd was formed in 83% yield as measured by integration against an internal integration standard (sealed capillary of Cp_2Co in C_6D_6).

Method B (from [L^{Me}FeCl]$_2$ and LiNHAd). [L^{Me}FeCl]$_2$ (1.1 g, 1.08 mmol) and LiNHAd (343 mg, 2.18 mmol) were stirred in pentane (40 mL) for 8 h. The brown mixture was filtered and concentrated under vacuum to 20 mL. The brown pentane solution was cooled to −35 °C, and yellow crystals of L^{Me}FeNHAd were isolated in good yield (1.2 g, 90%). ^{1}H NMR δ_H (C_6D_6): 125 (1, backbone), 98 (6, Me or Ad-α), 63 (3, Ad-β or Ad-γ), 41 (3, Ad-β or Ad-γ), 31 (3, Ad-β or Ad-γ), 19 (6, Me or Ad-α), −19 (4, *m*-Ar or C*H*(CH$_3$)$_2$), −36 (12, CH(CH_3)$_2$), −78 (2, *p*-Ar), −115 (12, CH(CH_3)$_2$), −125 (4, *m*-Ar or C*H*(CH$_3$)$_2$) ppm. ^{1}H NMR δ_H (THF-d_8): 70 (6, Me or Ad-α), 52 (3, Ad-β or Ad-γ), 31 (3, Ad-β or Ad-γ), 25 (3, Ad-β or Ad-γ), 12 (6, Me or Ad-α), −12 (12, CH(CH_3)$_2$), −16 (4, *m*-Ar or C*H*(CH$_3$)$_2$), −65 (2, *p*-Ar), −86 (12, CH(CH_3)$_2$), −96 (4, *m*-Ar or C*H*(CH$_3$)$_2$) ppm. UV/vis (pentane): 240 (15 mM^{-1} cm^{-1}), 300 (12 mM^{-1} cm^{-1}), 330 (14 mM^{-1} cm^{-1}) nm. μ_{eff} (C_6D_6, 25 °C): 4.8 ± 0.3 μ_B. Elem Anal. Calcd: C, 75.10; H, 9.21; N, 6.74. Found: C, 74.66; H, 7.55; N, 6.28.

L^{Me}Fe(AdNNNNAd) (5). We have previously shown that **5** is formed from $L^{Me}FeNNFeL^{Me}$ and 4 equiv of N_3Ad in the presence of *tert*-butylpyridine.[48] This compound can also be prepared from isolated **2**, or from $L^{Me}FeNNFeL^{Me}$ and N_3Ad in THF instead of *tert*-butylpyridine via the following methods.

Method A (From Isolated 2). A vial was loaded with **2** (19.2 mg, 30.8 μmol) and pentane (2 mL), giving a dark yellow-brown solution. A solution of N_3Ad (5.5 mg, 31 μmol) in pentane (1 mL) was added, and the resulting mixture was stirred for 2 h, during which the color changed to a dark olive-brown and a dark precipitate was evident. The mixture was cooled to −45 °C, and the olive-green precipitate was collected and washed with 3 mL of cold (−45 °C) pentane, affording spectroscopically pure **5** (19.2 mg, 78%).

Method B (From $L^{Me}FeNNFeL^{Me}$ in THF). A simpler procedure is given for the preparation of L^{Me}Fe(AdNNNNAd) without the use of *tert*-butylpyridine. A vial was loaded with $L^{Me}FeNNFeL^{Me}$ (61.4 mg, 63.0 μmol) and THF (5 mL) to give a royal purple solution. A solution of N_3Ad in THF (1 mL) was added, causing effervescence and a color change to dark yellow-brown. The reaction was stirred for 12 h, and the volatile materials were removed under vacuum. The residue was slurried in cold (−45 °C) pentane, and an olive-green powder was collected on a glass fritted funnel and washed with 5 mL of cold pentane to afford spectroscopically pure **5** (82 mg, 81%). Full characterization of this complex has been reported previously.[48]

X-ray Absorption Spectroscopy. XAS data were recorded at the Stanford Synchrotron Radiation Laboratory (SSRL) on focused beamline 9−3, under ring conditions of 3 GeV and 60−100 mA. A Si(220) double-crystal monochromator was used for energy selection, and a Rh-coated mirror (set to an energy cutoff of 10 keV) was used for harmonic rejection. Internal energy calibration was performed by assigning the first inflection point of the Fe foil spectrum to 7111.2 eV. The solid samples were prepared by dilution in boron nitride, pressed into a pellet, and sealed between 38 μm Kapton tape windows in a 1 mm aluminum spacer. The solution samples were prepared by dilution in toluene (~10−15 mM) and loaded into a Delrin XAS sample holder, with a 38 μm Kapton window. All samples were maintained at 10 K during data collection using an Oxford Instruments CF1208 continuous flow liquid helium cryostat. Data were measured in transmission and fluorescence mode (using a Canberra Ge 30-element array detector), respectively. XAS data were measured to k = 15 Å^{-1}. The data were calibrated and averaged using EXAFSPAK.[61] Pre-edge subtraction and splining were carried out using PYSPLINE.[62] A three-region cubic spline of order 2, 3, 3 was used to model the smooth background above the edge. Normalization of the data was achieved by subtracting the spline and normalizing the postedge region to 1. The resultant EXAFS was k^3-weighted to enhance the impact of high-k data. Theoretical EXAFS signals $\chi(k)$ were calculated using FEFF (version 7.0)[63] and fit to the data using EXAFSPAK.[62] The non-structural parameter E_0 was also allowed to vary but was restricted to a common value for every component in a given fit. The structural parameters varied during the refinements were the bond distance (R) and the bond variance (σ^2). The σ^2 is related to the Debye−Waller factor, which is a measure of thermal vibration and to static disorder of the absorbers/scatterers. Coordination numbers were systematically varied in the course of the analysis, but they were not allowed to vary within a given fit.

(59) (a) Ammann, C.; Meier, P.; Merbach, A. E. *J. Magn. Reson.* **1982**, *46*, 319–321. (b) Kaplan, M. L.; Bovey, F. A.; Cheng, H. N. *Anal. Chem.* **1975**, *47*, 1703–1705.

(60) (a) Baker, M. V.; Field, L. D.; Hambley, T. W. *Inorg. Chem.* **1988**, *27*, 2872–2876. (b) Schubert, E. M. *J. Chem. Educ.* **1992**, *69*, 62.

(61) George, G. N. *EXAFSPAK*, Stanford Synchrotron Radiation Laboratory, Stanford Linear Accelerator Center, Stanford University: Stanford, CA.

(62) Tenderholt, A. *PySpline*, Stanford Synchrotron Radiation Laboratory, Stanford Linear Accelerator Center, Stanford University: Stanford, CA.

(63) (a) Mustre de Leon, J.; Rehr, J. J.; Zabinsky, S. I.; Albers, R. C. *Phys. Rev. B* **1991**, *44*, 4146–4156. (b) Rehr, J. J.; Mustre de Leon, J.; Zabinsky, S. I.; Albers, R. C. *J. Am. Chem. Soc.* **1991**, *113*, 5135–5140.

Magnetic Susceptibility. Magnetic susceptibility data were measured from powder samples of solid material in the temperature range 2−300 K by using a SQUID susceptometer with a field of 1.0 T (MPMS-7, Quantum Design, calibrated with standard palladium reference sample, error $<2\%$). Multiple-field variable-temperature magnetization measurements were done at 1 T, 4 T, and 7 T with the magnetization equidistantly sampled on a $1/T$ temperature scale. The experimental data were corrected for underlying diamagnetism by use of tabulated Pascal's constants,[64] as well as for temperature-independent paramagnetism. The susceptibility and magnetization data were simulated with our own package julX for exchange coupled systems.[65] The simulations are based on the usual spin-Hamilton operator for mononuclear complexes:

$$\hat{H} = g\beta\hat{\vec{S}}\cdot\vec{B} + D[\hat{S}_z^2 - 1/3S(S+1) + E/D(\hat{S}_x^2 - \hat{S}_y^2)] \quad (1)$$

where S is the total spin, g is the average electronic g value, and D is the axial zero-field splitting parameter, and E/D is the rhombicity of the zero-field splitting. Diagonalization of the Hamiltonian was performed with the routine ZHEEV from the LAPACK Library, and the magnetic moments were obtained from first order numerical derivative dE/dB of the eigenvalues. Intermolecular interactions were considered by using a Weiss temperature, Θ_W, as perturbation of the temperature scale, $kT' = k(T-\Theta_W)$ for the calculation. Powder summations were done by using a 16-point Lebedev grid.

Computational Details. All computations employed the Gaussian03 suite of programs.[66] Whether quantum (truncated models) or hybrid quantum/classical (full experimental models) simulations, all calculations utilize the B3LYP hybrid density functional[67] and the extended Pople basis set, 6-311+G(d), which incorporates diffuse and polarization basis sets on main group elements, and an f-polarization function on iron.

For the QM/MM calculations, the classical region (Universal Force Field) contained the 2,6-diisopropylphenyl and methyl substituents of the β-diketiminate ligand and the adamantyl group with the exception of the carbon that is directly bonded to nitrogen. The remainder of the complex was modeled at the B3LYP/6-311+G(d) level of theory. The ONIOM methodology of Morokuma and co-workers was used for all quantum/classical hybrid simulations.[68]

All open shell species were modeled within the unrestricted Kohn−Sham formalism. Inspection of total spin expectation values suggested some degree of spin contamination for the quartet states, so results should be viewed with this caveat. All models (full and truncated) were geometry optimized without symmetry constraint using gradient methods. The energy Hessian was evaluated at all stationary points to designate them as either minima or transition states at the pertinent levels of theory. Reported free energies are at 298.15 K and 1 atm and are calculated with unscaled vibrational frequencies.

Acknowledgment. The authors acknowledge financial support from the Petroleum Research Fund (44942-AC to P.L.H.), the Department of Energy (DE-FG02-03ER15387 to T.R.C.), the National Science Foundation (CHE-0911314 to P.L.H.; Graduate Research Fellowship to R.E.C.), and the Department of Chemistry and Chemical Biology at Cornell University (S.D.). SSRL operations are funded by the Department of Energy, Office of Basic Energy Sciences. The Structural Molecular Biology program is supported by the National Institutes of Health, National Center for Research Resources, Biomedical Technology Program and by the Department of Energy, Office of Biological and Environmental Research. Calculations employed the UNT computational chemistry resource, for which T.R.C. and N.J.D. acknowledge the NSF for support through CRIF Grant CHE-0741936. We thank Dr. William Brennessel for assistance with X-ray crystallography.

Supporting Information Available: Spectroscopic and crystallographic details, additional computational results, compiled data from the Cambridge Structural Database, and full list of authors for ref 66. This material is available free of charge via the Internet at http://pubs.acs.org.

(64) (a) O'Connor, C. J. *Prog. Inorg. Chem.* **1982**, *29*, 203–283. (b) Weast, R. C.; Astle, M. J. *CRC Handbook of Chemistry and Physics*, CRC Press Inc., Boca Raton, FL, 1979.

(65) Available from E.B.: http://ewww.mpi-muelheim.mpg.de/bac/logins/bill/julX_en.php

(66) Frisch, M. J. et al., *Gaussian 03, Revision D.02*, Gaussian, Inc., Wallingford CT, 2004.

(67) (a) Becke, A. D. *J. Chem. Phys.* **1993**, *98*, 5648–5652. (b) Lee, C.; Yang, W.; Parr, R. G. *Phys. Rev. B* **1988**, *37*, 785–789.

(68) Svensson, M.; Humbel, S.; Froese, R. D. J.; Matsubara, T.; Sieber, S.; Morokuma, K. *J. Phys. Chem.* **1996**, *100*, 19357–19363.